Journal of the Indian Institute of Science
A Multidisciplinary Reviews Journal
ISSN: 0970-4140 Coden-JIISAD

REVIEWS

Models and Mechanisms of Oxygen Evolution Reaction on Electrocatalytic Surface

Sulay Saha, Koshal Kishor, Sri Sivakumar[1,2] and Raj Ganesh S. Pala[2]

Abstract | A profound change has taken place in understanding surface electrochemistry during water-splitting reaction due to the accumulated knowledge over the past decades and supported by recent advances in spectroscopic techniques and high-performance quantum chemical simulations. The design of electrocatalysts has been improved due to better understanding of surface structures of electrocatalysts and their active sites. This review provides insights into both theoretical and experimental electrochemistry that are directed towards a better understanding of the rate-determining step of water splitting, i.e., oxygen evolution reaction (OER). The emphasis of this review is on the origin of the electrocatalytic activity of nanostructured catalysts toward the aforementioned reaction by correlating the electrode performance with their intrinsic electrochemical properties. Also, the design aspects of acidic- and alkaline-medium electrocatalysts is discussed from preliminary discussion on active site engineering to a more applied concern of achieving highly stable and active electrode fabrication. The design concerns while choosing a support for OER electrocatalyst has also been discussed. At the end, challenges in electrolyser designs and problems faced by the industry to commercialize the electrolyser in a cost-effective manner have been discussed.

1 Introduction

Generation of clean energy is one of the main issues of the 21st century because the use of the fossil fuels has problems associated with diminishing reserves and environmental compatibility.[1–7] An alternative source of the energy carrier can be hydrogen, which has high energy density and can also generate clean discharge (water) on burning.[5,6] Also, hydrogen is the most important chemical in chemical industry as petrochemical, fertilizer and semiconductor industry are significantly dependent on its supply.[8] However, pure hydrogen as a gas is scarce in the earth's environment and its demand is mainly met through steam-reforming of hydrocarbons, which generates CO and CO_2 as byproducts.[9] Electrochemical water electrolysis is another process, which can generate hydrogen.[10] Though this process does generate clean fuel, it is an energy-intensive limiting its industrial application.

Hydrogen is generated at the cathode and oxygen is generated at the anode during water electrolysis. The process involves oxidation (loss of electrons) at anode and reduction at cathode (protons accepting electrons, which come from the conducting wire) with the help of supporting electrolyte in aqueous medium. The generated hydrogen can be used as an industrial fuel, or for hydrogenation reaction as well as source of electricity when "burnt electrochemically" in a fuel cell. Generation of hydrogen through water electrolysis was preferred over steam-reforming until the flourishing of petrochemical industry with accompanying decrease in crude oil prices, which led to closure of many electrolysis plants. The upward trend in crude prices along with environmental concerns these petrochemical processes bring has led to relook of water electrolysis with increasing interest. The general efficiency of these electrolysis processes is around

Department of Chemical Engineering, Indian Institute of Technology, Kanpur, 208016, India.
[1]Materials Science Programme, Indian Institute of Technology, Kanpur, 208016, India.
[2]Centre for Environmental Science and Engineering, Indian Institute of Technology, Kanpur, 208016, India.
[2]Centre for Nanoscience and Soft Nanotechnology, Indian Institute of Technology, Kanpur, 208016, India.
srisiva@iitk.ac.in, rpala@iitk.ac.in

~80% and the lab-scale efficiency is around ~94% (See for definition of efficiency in equation 14). Since the whole electrolysis process is electrical energy-intensive due to inherent endothermic nature of the reaction, coupling the electrolyzer with a renewable energy source is being suggested to increase the viability of the electrolysis process. Among different energy sources that are coupled with water electrolyzers, steam[11], wind[12], solar[13,14] and geo-thermal energy[15] have been mainly explored. Also, instead of electrochemical hydrogen generation, photo-electrochemical hydrogen generation is also being tried and recently getting investigated in great detail.[16,17] Table 1 summarizes the different types of electrolyzers that are used in the industry and their efficiency.

Ideal water splitting requires 1.23 V potential at standard thermodynamic conditions. However, the activation barrier associated with the chemical reaction and ohmic loss leads to splitting of water at much higher potential. The hydrogen evolution (HER) at the cathode is a two-electron process and OER at the anode a four-electron process. It has been observed that OER at the anode is the rate-determining step and requires higher overpotential when compared to HER. Thus, the performance and efficiency of the water electrolysis cells is intricately related to the performance of OER electrocatalyst at the anode. Until the 1970s, expensive OER catalysts, made up of late transitional metal oxides (e.g., Ru, Ir), were generally used in the electrolyzers. This led to increase in cost of the overall process, making the whole process economically less viable. With the introduction of alkaline water electrolyzers[20] and invention of dimensionally stable anodes[21] in acidic medium in the 1980s, the focus of electrocatalysis research has shifted to finding active electrocatalysts via earth-abundant and cheap elements. The central issue is that while stable and active catalysts are made using expensive Noble materials like Ru, Ir, Pt, Pd, those made from earth-abundant and cheap material like Ni, Co, Fe have lower activity as well as suffer from corrosion. Thus, it is not only important to understand the reaction mechanism of electrochemical OER but also the associated dissolution reaction of anodes under electrochemical OER condition. Understanding of the reaction mechanism, identification of active and stable sites in electrocatalysts is greatly expected to help in the design of better electrocatalysts for the future.

This work summarizes the recent progress in the development of OER electrocatalysts in acidic and alkaline media. Since, both these electrocatalysts can be used in neutral medium and neutral medium electrolyzers show lower efficiency due to low ionic conductivity of water and do not have any limitations in electrocatalysts, they are not discussed in this review. Instead of focusing on catalyst preparation and its role in increasing the activity, we have paid attention to the nature of the active sites of electrocatalysts and their conditioning for designing superior electrocatalysts with better stability and activity. Fundamental aspects of the OER and its electrochemical aspects are also addressed particularly as well as practical requirements and benchmarking criteria while reporting OER electrocatalysts. Since the electrode comprises support also, we have discussed the design criteria for supports. However, we note that finding a better OER electrode is only one aspect of making an efficient electrolyzer and several additional aspects of water electrolysis must be studied, e.g., contact resistance, polymer exchange membranes.[22]

1.1 *Electrode kinetics and benchmarking of activity*

1.1.1 Electrode kinetics: An understanding of the reaction kinetics is of utmost importance in the design of a better electrolyzer. The reactions at both the cathode and anode are redox reactions

Table 1: Different kinds of electrolyzers using different sources of energy for hydrogen production by electrochemical water splitting (See equation 14 for the definition of efficiency).

Serial no.	Type of electrolyzer	Type of energy used	Efficiency (%)	Operating temperature
1	Alkaline	Electrical	80	60°C[18]
2	Acidic	Electrical	85	80°C[19]
3	Steam	Electrical and Heat	92	800–1000°C[11]
5	Photo-voltaic	Solar	90	105°C[14]
6	Wind	Wind	78%	80°C[12]
7	Geothermal	Geothermal	80	900°C[15]
8	Photo-electrochemical	Solar	13	65°C[16]

• Pressurized water is used in high-temperature electrolyzers.

$O + ne \rightleftharpoons R$ involving electrons. Nernst equation governs the thermodynamic potential for such a reaction. This equation correlates the electrode potential (E) with the concentration of the products and reactants:

$$E = E^o - \frac{RT}{nF}\left[\ln\left(\frac{C_R^*}{C_O^*}\right)\right] \quad (1)$$

Here, the term E^0 is the thermodynamic equilibrium potential of an overall reaction, R, the universal gas constant, T, the temperature, n, the number electrons associated with the reaction, F, the Faraday constant, and (C_R^*/C_O^*), the concentration of oxidized/reduced species in the system. The thermodynamic equilibrium potential is the minimum potential bias that is required for any electrochemical reaction to calculate using the following equation:

$$E_{eq} = \frac{\Delta G}{nF} \quad (2)$$

During electrochemical reaction, redox reaction occurs at both anode and cathode. The current density obtained from a specific reaction at a particular electrode (e.g., anode) is given by,

$$j_f = nFk_fC_o \quad (3)$$

where j_f and k_f are the current density and reaction rate constant, respectively. Here, a standard rate constant k^o and rate constant can be related with Arrhenious relationship by:

$$k_f = k^o \exp\left[-\alpha f\left(E - E^{o'}\right)\right] \quad (4)$$

where f is equivalent to F/RT and α is termed as transfer coefficient with value between 0 to 1, which can be found out by Marcus theory.[23–25]

The electrochemical reactions do not occur at equilibrium thermodynamic potential and certain excess potential is required to overcome the energy barriers involved in the activated processes correlated with specific reaction intermediates and this excess potential is known as overvoltage or overpotential in electrochemist's parlance. This overpotential is written as:

$$\eta = E_{eq} - E \quad (5)$$

Here, E_{eq} is the equilibrium electrode potential, and E, the real electrode potential. The overall current density at a particular overpotential of the reaction is correlated through the following relation,

$$j = j_o\left[\frac{C_o}{C_o^*}\exp(\alpha f\eta) - \frac{C_R}{C_R^*}\exp\left((1-\alpha)f\eta\right)\right] \quad (6)$$

where C_R^* and C_o^* are the bulk concentration of the reduced and oxidized species and j_o is known as the exchange current density of the reaction. The exchange current density is an important descriptor for electrochemical reaction and is indicative of the activation barrier of the reaction. If the electrochemical reaction is not diffusion limited, i.e., either the electrolyte bath is well stirred, or the reaction rate is slow, then the bulk and the surface concentration can be taken as approximately almost equal (i.e. $C_R = C_R^*$ and $C_o = C_o^*$). In such a situation, the above equation would reduce to an equation which is more famously known as the Butler-Volmer equation,

$$j = j_o\left[\exp(-\alpha f\eta) - \exp\left((1-\alpha)f\eta\right)\right] \quad (7)$$

According to the Butler-Volmer equation at small j_o, the reaction kinetics would be slow. The Butler-Volmer equation shows that current density at any overpotential is the summation of oxidation (forward) and reduction (backward) reaction occurring at electrode surface. At acertain overpotential the contribution from the backward reaction is almost zero and only forward reaction dominates and in that case, Butler-Volmer equation for OER is reduced to the following form,

$$j = j_o\left[\exp(-\alpha f\eta)\right] \quad (8)$$

$$\log j = \log j_o - \alpha f\eta \quad (9)$$

The above equation simply states that the generated current due to electrochemical reaction is exponentially linked to the overpotential in the absence of diffusion resistance imposed on reactants and this reaction is better known as the Tafel equation. The above equation can be written in the following form,

$$\eta = a + b\log j \quad (10)$$

where a and b are the Tafel constants ($a = \frac{2.3}{\alpha f}\log j_0$, $b = -\frac{2.3}{\alpha f}$). Tafel equation is valid for all electrochemical reactions and is useful in the analysis of electrochemical energy storage devices (fuel cell, battery and electrolyzer, etc.).[26–28]

1.1.2 Benchmarking parameters for electrocatalyst: The performance of an electrocatalyst is usually gauged from the other electrocatalysts by using two typical metrics, (i) apparent total electrode activity (e.g.,

current density expressed in $mA/cm^2_{geometric}$ or overpotential required to attain certain current density), which is the most important factor for device-oriented electrocatalyst design, and (ii) the intrinsic activity of each catalytic site (e.g., turnover frequency (TOF) or specific current density expressed in mA/cm^2_{ECSA}) and this metric is more useful for fundamental studies on catalyst design. Among other electrochemical metrics, Tafel slope, exchange current density (J_0) or charge-transfer resistance (R_{ct}) calculated using electrochemical impedance spectroscopy at a potential in Faradaic region are also used in comparing the activity of electrocatalyst and understanding the basic phenomena occurring at the electrode/electrolyte interface. Generally, the activity of OER electrocatalysts is benchmarked through metrics of (i) overpotential required to attain a current density of 10 $mA/cm^2_{geometric}$, and (ii) current density at an overpotential of 0.35 V.[29,30] To attain higher efficiency, a lower Tafel slope and higher current densities are desirable. Preparation of three-dimensional porous electrocatalyst is an effective strategy to enhance OER activity. In these electrodes, the number of active sites would be significantly larger than that may arise from geometrical surface area though almost neither electronic properties nor surface structure of active sites has been altered. To compare the increased surface area from the apparent geometrical surfacearea, the following metric named Roughness Factor (RF) is introduced.

$$Roughness\ Factor\,(RF) = \frac{Electrochemical\ surface\ area\,(ECSA)}{Geometrical\ surface\ area\,(GSA)} \qquad (11)$$

where RF can be as high as 500–4000 in a porous 3D electrode. Consequently, while assessing the activity of individual sites, it is imperative to normalize it by real surface area or the TOF is to be calculated. However, the key issue is the accurate measurement of the electrocatalytically active surface area (ECSA), which can reflect the total number of active sites on a given surface for a certain reaction. While for metals, either underpotential deposition (upd) hydrogen (H_{upd}) adsorption voltammetry[31] or CO stripping voltammetry[32] is widely used, it is not useful for metal oxides, especially for OER. The surface area calculated using BET does not reflect the ECSA and sometime differs by an order of magnitude.[33,34] For example, in ABO_3 pervoskite material, either A or B would be electrocatalytically active for OER, but BET measurement would show both of them as active sites.[35] Therefore, it is advisable not to use BET surface area for measuring specific activity of OER. Other methods include measurement of double-layer capacitance (c_{dl}) through cyclic voltammetry or impedance spectroscopy at non-Faradaic region and then correlating it with ECSA[36] by using the following equation,

$$ECSA = \frac{C_{dl}\, d}{\varepsilon_r \varepsilon_0} \qquad (12)$$

where c_{dl}, ε_o, ε_r and d are the double-layer capacitance electrical permittivity, relative electrical permittivity and distance between two layers, respectively (d = 10 A°).[37] However, the measurement of the interfacial double-layer capacitance is methodologically difficult due to the fact that some semiconducting and capacitive properties as well as the double-layer frequency dispersion has contribution towards total capacitance, leading to questions on the reliability of the computed value.[30,38–40]

In porous 3D electrodes, porosity is another useful parameter but it needs to be measured. The porosity observed in liquid solution under electrochemical conditions would differ from that measured through BET, which are more accurate for solid-gas-phase heterogeneous catalytic conditions. Trasatti *et al.* suggest that porosity calculation through electrochemical means mirror more porous conditions in solid-liquid solution catalysis.[45] They suggest that the total charge (q_t) and outer charge (q_o) of metal oxide can be calculated by integration of voltammograms at different scan rates. The voltammetric charge corresponding to the total surface area (q_t) can be calculated by plotting the reciprocal of q against the square root of the potential scan rate and then by extrapolation of the linear plots at $\nu = 0$. The values of outer charge (q_o) can be calculated from the extrapolation to $\nu \rightarrow \infty$ in the plot of q vs $\upsilon^{-0.5}$. The electrochemical porosity is measured as

$$Electrochemical\ porosity = \frac{q_t - q_o}{q_t} \qquad (13)$$

Apart from this, Tafel slope and exchange current density (J_0) are used for comparing the OER activities of the electrocatalysts. Though Tafel slope is widely used as performance metric of OER electrocatalyst, it cannot be used as a singular measure since electrocatalysts having the same Tafel slope and different J_0 would show different OER activity. For calculation of J_0, special care is required as the current axis is in logarithmic scale and small errors during extrapolation of Tafel slope or ohmic-drop correction may result in

Turnover frequency (TOF): Turnover frequency is the specific activity per active site per unit time for a given reaction under defined reaction conditions.

Electrochemical impedance spectroscopy: The electrochemical impedance spectroscopy is the technique in which the impedance of a system is measured after application of a small amplitude of excitation signal (potential or current) covering a wide range of frequencies. This spectroscopy often enables decoupling of complex sequence of coupled events involving electron transfer, chemical reaction, mass transfer etc. through a single measurement.

Faradaic region: The electrochemical potential regions where reactions occurs accompanied with electron transfer between reactant and product, are identified as Faradaic region.

Exchange current density: Exchange current density (J_0) is the theoretical current density at a zero overpotential for a specific reaction.

large errors in J_0 values. Also, the experimentally obtained current densities are dependent on various measuring conditions such as (i) scan rate, (ii) electrolyte concentration, and (iii) distance between electrodes. One of the alternative ways of benchmarking condition is potentiostatic measurement in which steady-state potential is applied or galvanostatic measurement in which steady-state current density is maintained for a fixed time limit, say 1 h. The steady-state current density after a particular time gives a measure of activity while the reduction in current density after a fixed time is indicative of the stability of electrocatalyst. In this way, both activity and stability of different electrocatalysts can be measured.

One must note that the current density obtained in electrochemical OER conditions does not fully correspond to OER. It includes contribution from (i) dissolution current of electrocatalyst, (ii) pseudo-capacitive current, (iii) current arising from surface reconstruction the electrocatalyst, and (iv) other possible electrochemical reactions due to interaction with anions of supporting electrolyte, particularly in acidic conditions. Predominance of one of these above phenomena during OER condition would lead to wrong conclusion over electrocatalyst performance. Hence, it is better to calculate the Faradaic efficiency of OER through actual O_2 gas collection or measurement of O_2 concentration through in-situ spectroscopy.[41] The Faradaic efficiency is given as

$$\textit{Faradaic efficiency} = \frac{\textit{Experimentally collected total volume of oxygen gas}}{\textit{Theoretical amount of oxygen gas should evolve}} \times 100\% \quad (14)$$

Overall, depending on the electrocatalyst material, one should decide the benchmarking conditions they would choose.

2 Molecular Mechanisms in Oxygen Evolution Reaction

2.1 *Mechanistic pathway of OER*

It is essential to understand the mechanistic pathway and reaction barriers associated with OER for designing a better electrocatalyst. With the advent of density functional theory (DFT)-based simulations, it has become far easier to (i) discover new reaction mechanistic pathways for reactions,[42–45] and (ii) reveal active sites of catalysis,[45–48] which may help in the design of better catalysts.[49] These active sites are generally under coordinated surface sites of the electrocatalyst, which interact with reactants to form different reaction intermediates. Using DFT methodology, the energy of the possible reaction intermediates is calculated and the lowest activation barrier pathway is identified as the reaction pathway. The highest energy barrier reaction step of the lowest energy pathway is identified as the activation barrier with the reaction step identified as the rate-determining step.

The mechanistic pathway of OER on catalyst surface is dependent on electrochemical potential and surface coverage. Previously, it was believed that OER follows Langmuir-Hinshelwood mechanistic pathway involving neighboring active sites.[50] Bockris *et al.* suggest the following mechanistic pathway (Figure 1)[50],

$$S + H_2O \rightarrow S - OH + H^+ + e^-$$
$$S + OH \rightarrow S - O + H^+ + e^-$$
$$2S - O \rightarrow 2S + O_2$$

where S is the active site. The existence of this reaction pathway for OER has been proved by isotope-labelling studies for RuO_2 electrocatalyst.[51] With the advent of more powerful experimental spectroscopic and computational facilities, another parallel pathway involving OOH intermediate was proposed by Norskov *et al.*[52] The elementary reaction of this mechanistic pathway is as follows,

$$S + H_2O \rightarrow S - OH + H^+ + e^-$$
$$S - OH \rightarrow S - O + H^+ + e^-$$
$$S - O + H_2O \rightarrow S - O - OH + H^+ + e^-$$
$$S - O - OH \rightarrow S + O_2 + H^+ + e^-$$

where S is the active site. The schematic pathway of this mechanism for RuO_2 is given in Figure 2.

The preferred mechanistic pathway depends on the hydroxyl coverage over the active catalyst, which in turn is dependent on the electrochemical potential.[53] At lower electrochemical potential, –OH coverage is found to be more in comparison to –O coverage. In this zone, –OOH formation pathway is favored. With increase in electrochemical potential, –OH coverage over the surface is reduced and interaction between two neighboring –O adsorbates becomes possible thus making Langmuir-Hinshelwood mechanistic pathway plausible.

Due to the presence of these two mechanistic pathways, the rate-determining step for OER differs depending on the electrochemical potential applied. This is reflected in the switch of Tafel slopes commonly observed during OER.[54,55] At lower overpotential, it is common to observe a Tafel slope < 120 mV/dec, while at higher overpotential a Tafel slope of > 120 mV/dec is observed.

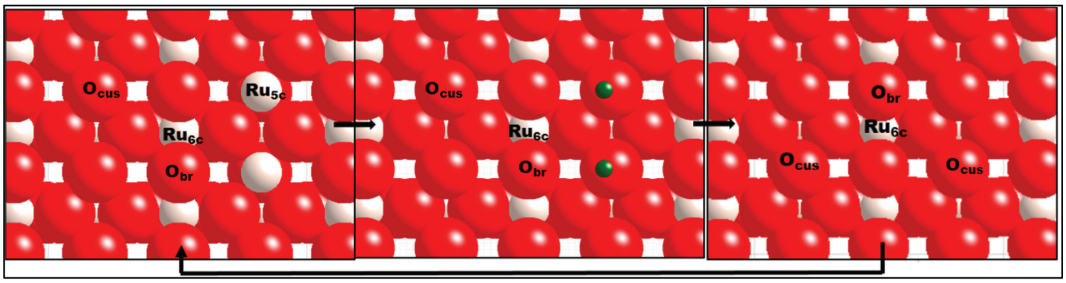

Figure 1: (Left) The ground state of oxygenated RuO_2 (110) surface with neighboring Ru-5c sites are open for –OH adsorption, (Middle) oxygenated RuO_2 (110) with neighboring dual $–OH_{cus}$ occupancy, (Right) oxygenated RuO_2 (110). The grey, red and green balls correspond to Ru-, O- and H-atoms, respectively. The arrows indicate the pathway of OER over RuO_2 (110) as proposed by Bokris *et al.*[50]

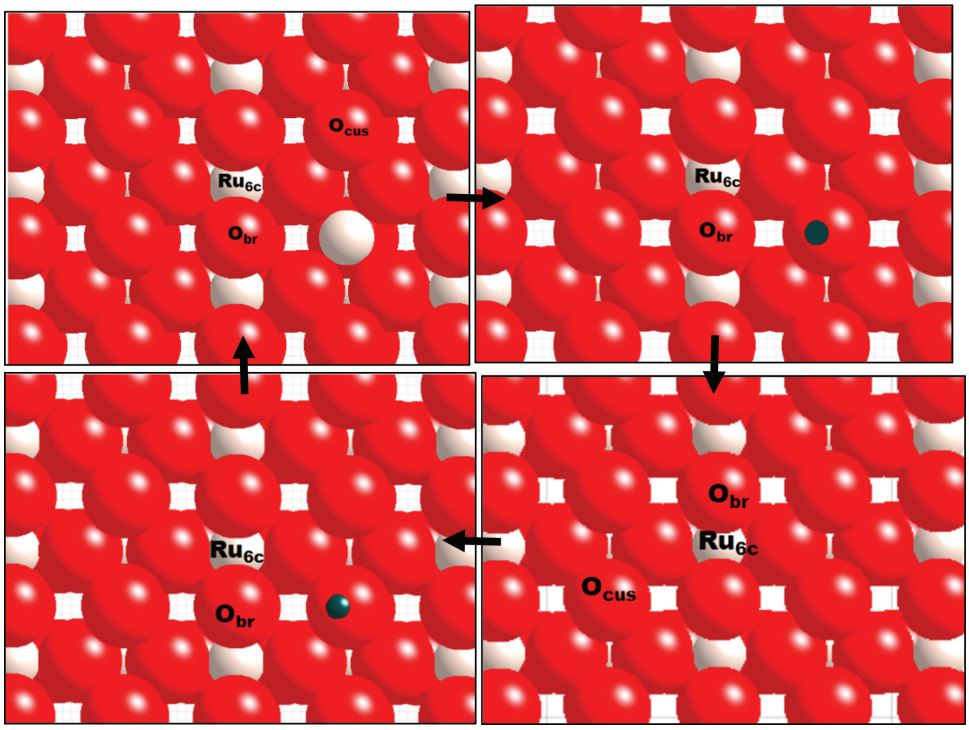

Figure 2: (Top left) The ground state of oxygenated RuO_2 (110) surface Ru-5c sites is open for –OH adsorption, (Top right) oxygenated RuO_2 (110) with a single $–OH_{cus}$ occupancy, (Bottom right) oxygenated RuO_2 (110) and (Bottom left) oxygenated RuO_2 (110) with $–OOH_{cus}$ occupancy. The grey, red, and green balls correspond to Ru-, O- and H-atom, respectively. The arrows indicate the pathway of OER over RuO_2 (110) as proposed by Norskov *et al.*[48,52]

Also, the mechanistic pathway differs depending on the oxide surface. As for example, RuO_2 (110) surface is found to show peroxide formation as a rate-determining step as it is far more easier to oxidize Ru-5c sites on (110) the surface compared to Ru-6c.[52] However, the rate-determining step of TiO_2 (110) surface is found to be different and is found to be the adsorption of oxygen adsorbates over Ti-5c sites as it is far more harder to oxidize Ti-5c sites on (110) surface compared to Ti-6c.[52] Also, in the same material, different surfaces behave differently depending on the electrochemical potential. This is exemplified in the case of Co_3O_4 through DFT studies by Santen *et al.*[46] At lower electrochemical potential, the most active surface is found to be (001) surface with the rate-determining step being the desorption of O_2 with the involvement of dual Co surface sites and Langmuir-Hinshelwood dominating the mechanistic pathway. But as the electrochemical potential is increased, the structure-sensitivity of other surfaces comes into play and (311) surface is found to be more active with the formation of –OOH as the rate-determining step. The lowering

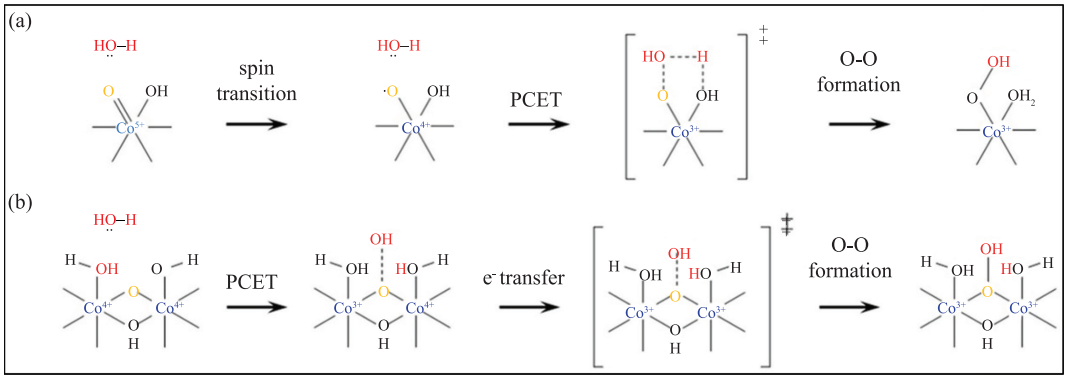

Figure 3: Mechanism of water adsorption to (a) a terminal Oxo on a single-Co Site, and (b) a bridging Oxo on a dual-Co Site at different points along the reaction trajectory. PCET stands for proton-coupled electron transfer. The figure is adapted from American Chemical Society.[46]

of activation barrier due to the involvement of two Co (IV) sites instead of a single Co (V) site during OER leads to the formation of a bridged intermediate having lower potential energy (Figure 3). The delocalization of holes around dual sites is also responsible for the lowering of potential energy. Further increase in electrochemical potential leads to single Co-site of (110) surface as the most active one. Similar results are obtained in the case of RuO_2, where OER activity between single-crystal-cut (100) and (110) surfaces are compared, and (100) surfaces are more active in comparison to (110) surfaces.[56] This type of structure sensitivity is due to interaction between neighboring sites and higher density of active metal sites per geometrical surface area.

It is being observed that surface metallic sites get oxidized to a higher oxidation state during OER ($M^n \rightarrow M^{n+m}$). If the chemical potential of surface oxides with higher oxidation state is lower than the chemical potential of bulk oxides with lower oxidation state in aqueous medium under electrochemical OER conditions, then the dissolution of electrocatalyst takes place, which seriously hampers the performance of electrolyzer in the long run.[57] For example, RuO_2 undergoes dissolution to RuO_4 with loss of activity under a potential of E > 1.4 V in aqueous medium.[58]

$$RuO_2\ (s) + 2H_2O\ (l) \rightarrow RuO_4\ (s) + (4H^+ + 4e^-)$$

Similar dissolution has been observed in the case of MnO_2 with generation of MnO_4^- species in aqueous medium,[49]

$$MnO_2\ (s) + 2H_2O\ (l) \rightarrow MnO_4^- + 4H^+ + 3e^-$$

This dissolution reaction occurs in parallel with OER. In an ideal OER electrocatalyst, the dissolution reaction would be suppressed without affecting the OER kinetics. However, the intermediates of dissolution reaction of electrocatalyst and OER are identical in most of the cases, which makes increasing OER activity over dissolution reaction hard to achieve.[59,60] Current research and developments on OER electrocatalyst are focused on enhancing OER activity, while suppressing the dissolution of electrocatalyst to electrolytes.[49,61] The current method of suppressing electrocatalyst dissolution into electrolytes involves preparation of doped/alloyed oxide or solid solution involving stable oxides (e.g., mixing stable TiO_2 with active RuO_2). However, lack of understanding of dissolution mechanism of electrocatalysts has made development and design of stable electrocatalyst largely empirical in nature.

2.2 *Origin of volcano plot and its utility in catalyst design*

OER reaction involves 4-electron transfer with the formation of various reaction intermediates. Ideally each electron transfer would require the same amount of energy. However, variation in the requirement of energies due to energetics of reaction intermediates imposes activation barrier for the reaction. For designing a better catalyst, Sabatier principle is recalled, which states that the catalyst should bind the reaction intermediates not too weakly or nor too strongly so that adsorption and desorption kinetics becomes faster.[62,63] In the case where the intermediates bind too weakly, they cannot activate the surface leading to lower activity. However, when they bind too strongly, all available surface sites are occupied leading to poisoning and desorption is difficult. Hence, moderate binding energies of intermediates on catalyst surface are a good compromise between these two extreme situations.

To understand the reaction kinetics better, a number of 'descriptors' are used and they are plotted against the actual activity of electrocatalysts. These descriptors are derived from the binding energies of adsorbates on the electrocatalyst surface. The binding energy of –OH, –O and –OOH adsorbates on the electrocatalyst surface vary between 0 and 5 eV. Plotting of activity against descriptor results in generally "volcano"-shaped correlation (Figure 4) and further, such descriptors are used for predicting the activity of an unknown material.

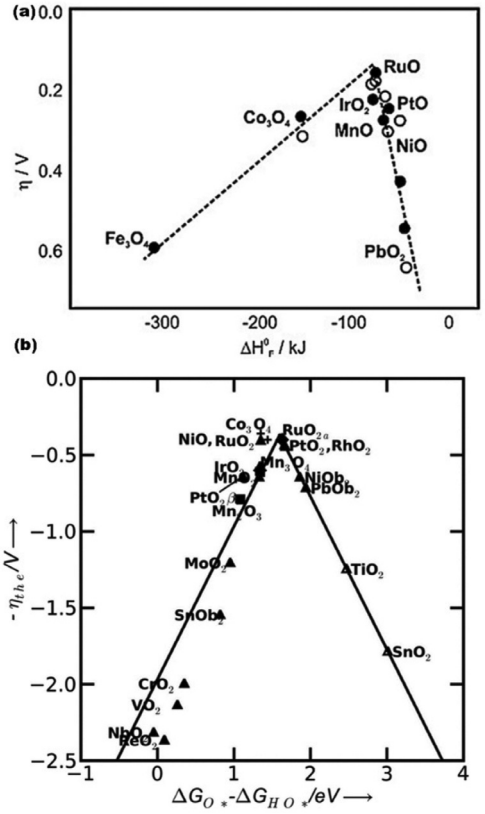

Figure 4: (a) Overpotential of binary oxides reported by Trasatti as function of the enthalpy of transition from a lower to a higher oxidation state. Measurements in alkali are shown as open symbols and those in acid as filled symbols. The figure is reproduced with permission from Elsevier.[64] (b) Activity trends towards OER for rutile, anatase, Co_3O_4 and Mn_xO_y oxides. The negative values of theoretical overpotential are plotted against the standard free energy of ($\Delta G_{HO^*} - \Delta G_{O^*}$) step. The effect of interaction with the oxygen from the neighbouring site is considered: rutileoxides (~), Mn_xO_y (&). For NiO_{b2}, PbO_{b2}, and SnO_{b2}, cus sites are empty, and the reaction takes place on the bridge sites of the surface. Hollow triangles (~) represent the low coverage regime. The figure is reproduced on permission from Wiley.[48]

Trasatti *et al.* suggest enthalpy of formation of oxides from a lower oxidation state to higher oxidation state as a descriptor ($M^nOx \rightarrow M^{n+m}Oy$) and plotting this energy against the activity of electrocatalyst resulted in a "volcano plot" (Figure 4a).[64–66] It is suggested that OER can be simply viewed as a transition between lower to higher oxidation state during adsorption of reactant water molecule and a transition between higher to lower oxidation state during desorption of O_2 gas molecule. As a result, metal oxides that are hard to be further oxidized would not be a good catalyst since reaction intermediates are weakly adsorbed. In these cases, water dissociation over catalyst surface would be the rate-determining step (e.g., TiO_2). On the reverse, oxides that are easily oxidized further would not be catalytically active since intermediates are strongly adsorbed and desorption of O_2 would be the rate-determining step (e.g. OsO_2). Later, Norskov *et al.* correlated OER reactivity with difference in the formation energy of oxide intermediate (–O) and hydroxyl intermediate (–OH) due to reaction of adsorbate-free surface and H_2O molecule (Figure 4b).[48,52] This descriptor works well for various oxide surfaces such as rutile, pervoskite, spinel, rock salt, and bixbyite.[48] Regardless of the quality of electrocatalyst material, the above descriptor imposes an overpotential limitation of 0.4 V for OER and this corresponds to the peak of the volcano.[48] However, this imposed limitation is not sacrosanct and can be circumvented by changing the nature of active sites.[67,68] Rossmeisl *et al.* showed through DFT simulation that OER on Ni- and Co-doped RuO_2 electrocatalyst has proton donor–acceptor functionality on otherwise inactive under coordinated oxygen sites at the surfaces, which enhance the surface reactivity at under coordinated (cus) Ru (–5c) sites by reducing the formation energy of –O and –OOH reaction intermediates.[67] This is also reflected experimentally as Ni-doped RuO_2 is far more active than conventional RuO_2 as predicted from volcano relationship.

While designing an electrocatalyst with doped oxide or alloy of an oxide, the target is to ascend towards the peak of the volcano. To achieve this, the general design principle is to combine materials from different legs of the volcano curve as a synergistic effect is expected. However, it has to be kept in mind that energetics of doping follows its own rule and dopant in doped oxide might not occupy the active sites due to thermodynamic conditions during synthesis. This is especially true for aliovalent and guest-host size-mismatched dopants, where surface segregation and undesirable defect formation is quite common.[69]

Usually, the free energy and related quantities for intermediates formed in oxygen-involving reactions on various surfaces change are correlated. This phenomenon has been observed for different surfaces including metals and metal oxides and is known as a scaling relationship between the oxygen intermediates.[48,52,70,71] Specifically, in the case of metal surfaces and transition metal oxides, the lines corresponding to –OOH and –OH are almost parallel to each other with the slope of one, as shown in Figure 5. The underlying principle for such behaviour is that the adsorbates, –OOH and –OH, form single bond with the catalyst surface through an oxygen atom via a single bond while –O forms double bond with the catalyst surface. This is reflected in the slope of formation energy of –O intermediate vs –OH intermediate which is nearly 2 (i.e. $\frac{\Delta G_O}{\Delta G_{OH}} = 2$).[48] Although surface-adsorbate scaling relationships provide qualitative arguments for tuning catalytic activity based on the bond strength between catalyst surface and adsorbate, they provide only a limited guideline for prediction of OER activity with increasing/decreasing coordination in lattice or change of elements, which can further help in the search for better catalyst. In this regard, the relationship between the surface adsorbate, binding strength and the electronic band structure has to be investigated for engineering better catalysts. The electronic structure of d-bands of transition metal surfaces was found to have a correlation with chemisorption energies for adsorbates on the surfaces and is useful for both explanatory and predictive tool in the catalysis.[72–78] In metal oxides, metal 3d-band splits into two kinds of electronic states: with doubly degenerate$_g$ symmetry and triply degenerate t_{2g} symmetry. It is found that there exists a correlation between adsorption energies and the occupancy level of t_{2g} orbital. Since the e_g and t_{2g} orbitals are normally nonbonding or antibonding and the 2p orbitals of oxygen are the bonding orbitals in octahedral complexes, an increase in the number of outer electrons in transitional metal would correspond to a weakening of the binding strength while interacting with electrophilic adsorbates (–OH, –O, –OOH). Distortions to the octahedral symmetry of the metal cation coordination structure lead to changes in both the shape of the t_{2g}-band and adsorption energy which lead to changes in OER activity. Also, the binding strength of atomic oxygen adsorbate on surfaces of metal oxides can be correlated to lattice oxygen atoms' p-band centre in a metal oxide.[76] Also, the p-band centre position scales are found to vary linearly with oxygen vacancy formation energy and oxygen surface exchange kinetics.[76] Though these scaling relations are helpful in understanding some of the features of catalyst design, it is important to recognize their limitations. While the predicted trend provides insight into understanding the difference in OER activity across different electrocatalysts, these relations are applicable for surfaces that follow a similar reaction mechanism. Change in reaction mechanism may result in change in the scaling relations with breakdown of volcano relations.

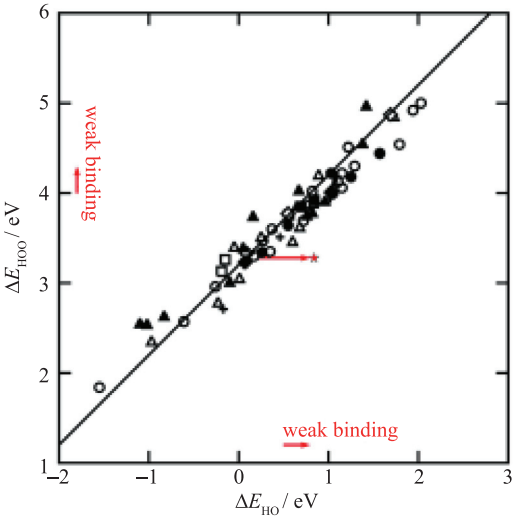

Figure 5: Adsorption energy of –OOH adsorbate plotted against the adsorption energy of –OH adsorbate on catalyst surfaces for perovskites, rutiles, anatase, Mn_xO_y, Co_3O_4, and NiO oxides. These calculations do not include zeropoint energy and entropy corrections. Hollow symbols represent the adsorption energy on the clean surfaces: perovskites (○), rutiles (Δ), Mn_xO_y (□), anatase (◊), Co_3O_4 (+), NiO. The solid symbols represent the adsorption energies on high coverage surfaces, with oxygen atoms representing nearest neighbors. The red star indicates the point at which the binding energies need to be for an ideal electrocatalyst. The above figure is published with permission from Wiley.[48]

2.3 *Nature of electrocatalyst-electrolyte interface*

An aspect worth considering but is often disregarded during computational catalyst design is the nature of the electrocatalyst–electrolyte interface during electrochemical OER conditions. Oxides having metallic electronic conductivity results in lower ohmic drop in the electrode bulk material. Among oxides, RuO_2, IrO_2 and $LaNiO_3$ show quasi-metallic electronic conductivity. However, most of the other transition metal oxides used for OER are semiconducting in nature which

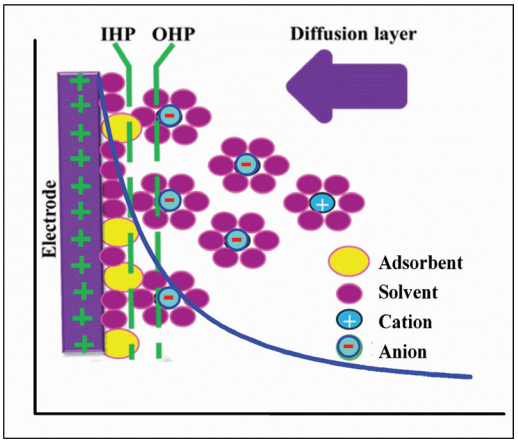

Figure 6: A schematic of the electrode-electrolyte interface is shown. The surface of the electrode is hydrated in addition to H_2O molecule, other types of adsorbents such as –OH, –O, –OOH and anions of electrolytes. In addition to H_2O, electrolyte ions get oriented due to localized charges on the surface. Cations are hydrated in the solution. The centre of the closest charge layer, the adsorbed layer, is defined as the inner Helmoltz plane (IHP), which is about 0.2 nm thick, while the outer Helmoltz plane is defined by the centre of the closest hydrated ions that can approach the surface, which is about 0.5–0.7 nm thick. In the diffuse layer the ion concentration is greater than that found in the bulk of the electrolyte medium.

adds to ohmic drop in electrode, thereby affecting the overall efficiency.

When a metal/semiconductor electrocatalyst comes into contact with an electrolyte, an electrical double layer is formed (Figure 6). Compared to metals, semiconductors provide much lower concentration of charge-carrier leading to formation of a large space charge layer at the surface. In general, p-type semiconductor exhibits low potential drop in the space charge layer due to the accumulation of holes at the surface in electrochemical OER conditions. However, an additional barrier for charge carriers is formed in the space charge layer at the interface of n-type semiconductors.[34] Hence, metallic or p-type semiconductor oxides would be more suitable electrocatalysts than n-type semiconductors as anodic electrocatalysts.

3 Electrocatalytic Materials for Oxygen Evolution Reaction

3.1 *OER electrocatalyst for PEMWE*

3.1.1 Monometallic oxides: The electrochemical splitting of water performed in acidic polymer electrolyte membrane water electrolysers (PEMWEs) has several distinct advantages compared to that of alkaline systems as discussed in earlier sections. The main challenge here is to design a cost-effective, and active but stable electrocatalyst in acidic medium. Only a small number of metallic oxides are stable in the acidic medium (see Table 2), which restricts the manoeuvrability in designing superior catalysts. The experimentally observed overpotential sequence for OER in acidic solution is as follows: Ru < Ir < Pd < Rh < Pt < Au, while the stability order is Pt ~ Pd < Ir < Rh < Au ~ Ru.[79,80]

The above relation is true for sputtered thin film oxides and both their activity and stability can be tuned through engineering of electrocatalyst surfaces via different synthesis conditions. For example, RuO_2 (100) surface is more stable and active than RuO_2 (110).[56] Therefore, both theoretical and experimental results for OER catalysts should be analysed with due care since the former study only considers ideal surfaces and the latter provides results strongly influenced by the catalyst preparation process and surface state. Also, crystallinity of prepared electrocatalyst also affects the electrocatalytic activity due to defect formation and surface stress. The activity ordering is found to be: amorphous RuO_2 > polycrystalline RuO_2 > single crystal RuO_2, while the stability is inverse of this order.[81,82]

The evolution of RuO_2 surface structure has been a subject of much interest.[55,60,79,83,84] In-situ XANES study of Ru-electrode revealed that under 0 < E < 0.8 V RHE potential Ru-remains in metallic state, between 0.8 < E < 1.0 V RHE potential the oxidation state is between 3 and 4, under 1.0 < E < 1.3 V RHE rutile oxide is formed with oxidation state of 4 and above E > 1.4 V potential, the oxidation state is higher than 4.[83] Prior to OER, it has oxidation state of 6 and with its onset its oxidation state increases to 8. RuO_2 undergoes dissolution mainly as RuO_4. Though corrosion rate increases with onset of OER, small amount of dissolution is observed even below OER. As expected, the dissolution rate is expected to depend on the stability of the intermediates formed during OER and dependent on the crystallinity, defects and the nature of the exposed surface which is again dependent on the synthesis process.

Besides RuO_2, another very active OER electrocatalyst in acidic medium is IrO_2. Though it is expensive and its electrocatalytic activity towards OER is inferior to RuO_2, its stability in high anodic potentials in acidic environment makes it attractive.[79,85] As in RuO_2, both the activity and stability of IrO_2 can be tuned through controlling the exposed facet in the surface, crystallinity and defect formation, which are again dependent on the

Table 2: Stability of the mono-elementary oxides in acidic medium under electrochemical OER conditions. The yellow color denotes formation of unstable oxide and green that of stable oxides. Blue color denotes the presence of two types of oxides under different electrochemical potential.

H																	He
Li	Be											B	C	N	O	F	Ne
Na	Mg											Al	Si	P	S	Cl	Al
K	Ca	Sc	Ti	V	Cr	Mn	Fe	Co	Ni	Cu	Zn	Ga	Ge	As	Se	Br	Kr
Rb	Sr	Y	Zr	Nb	Mo	Tc	Ru	Rh	Pd	Ag	Cd	In	Sn	Sb	Te	I	Xe
Cs	Ba	La-Lu	Hf	Ta	W	Re	Os	Ir	Pt	Au	Hg	Tl	Pb	Bi	Po	At	Rn
Fr	Ra	Ac-Lr	Rf	Db	Sg	Dh	Hs	Mt	Ds	Rg	Cn	Uut	Uuq	Uup	Uuh		
		La	Ce	Pr	Nd	Pm	Sm	Eu	Gd	Tb	Dy	Ho	Er	Tm	Yb	Lu	
		Ac	Th	Pa	U	Np	Pu	Am	Cm	Bk	Cf	Es	Fm	Md	No	Lr	

synthesis procedure.[56,86–88] Ir-metal also undergoes change in surface oxidation state similar to Ru but the potentials are higher than that of Ru.[89] Even at high potential of 1.95 V RHE, sputtered IrO_2 catalyst shows no corrosion.[90]

3.1.2 Doped and alloyed oxides: The idea of synthesising mixed oxide electrocatalysts is to introduce synergistic effect of both components and climb uphill in the volcano curve. To enhance the stability of RuO_2, the general strategy is to mix it with stable oxides even if they are passive oxides such as IrO_2, CeO_2, SnO_2, TiO_2.[55,61,91–95] Like RuO_2, these oxides possess rutile structures (e.g., IrO_2, CeO_2, SnO_2, TiO_2) but have high overpotential for the OER as well as lower electrical conductivity, which makes them a poor choice if they are used as stand-alone OER electrocatalysts. However, when these oxides are mixed with RuO_2, the current density is higher than separate phases of individual oxides and the solid solution has greater stability.[61,92,93] On detailed surface study after prolonged galvanostatic treatment of RuO_2–IrO_2 catalyst, the surface contains almost no Ru, but still its activity is higher.[93] This is attributed to the pure Ir surface skeleton arising due to surface Ru-dissolution that now contains higher number of steps and kinks which might be having greater activity than planar surface and higher density of active sites per geometrical surface area. The DFT simulation study of OER in defective surfaces of electrocatalyst has not yet been investigated.

Similar increase in activity is also observed in RuO_2–TiO_2 electrocatalyst, which is generally known as dimensionally stable anode. Naslund *et al.* suggest that the increase in activity due electron transfer from Ru to Ti site, which activates otherwise benign Ti atoms.[92] Indeed, the increased activity is achievable with Ru concentration in the doped oxide as low as 30%. DFT simulation suggests that activity of Ru surface atom on TiO_2 (110) surface does not get affected due to change in the neighboring environment.[96] However, the activation barrier for neighboring Ti-atoms gets reduced due to distortion of surface in the presence of bigger Ru-atom.[97] Yet, the activation barrier for OER for Ti surface dopants in RuO_2 almost remains unaffected. Hence, it is more beneficial to dope Ru on TiO_2 matrix. One other way of activating these electrocatalysts further is to introduce another dopant, which may activate the TiO_2 electrocatalyst. Lower-valent cations such as Ni, Co and Zn have been found to activate both RuO_2 and TiO_2 individually for OER even beyond volcano limitations as found through both experimental and simulation.[61,68,96,98–101] Additionally, these aliovalent dopants improve charge transfer behavior through formation of oxygen vacancy in bulk electrocatalyst, which result in improved conductivity in addition to lowering activation barrier for OER through strain and electronic effects. These non-Noble dopants are unstable in acidic medium and their dissolution would generate porous electrocatalyst as well as higher number of kinks, steps, and defects on the surface (see Figure 7). Indeed Pala *et al.* showed that the OER activity of Zn-doped RuO_2–TiO_2 electrocatalyst increases with electrochemical cycling and time.[61] This is also accompanied by an increase in ECSA and electrochemical porosity. Additionally, this is achieved without compromising stability and also reducing the cost of electrocatalyst. This can be a model for generating porous, active and stable electrocatalyst for acidic conditions. However, the intrinsic specific activity of generated active sites of this type of electrocatalyst is yet to be investigated.

Search for activated cheap electrocatalyst resulted in further research on activating TiO_2 electrocatalyst, which is stable in acidic medium and good for photo-electrocatalysis[102,103] but performs poorly as an electrocatalyst due to its n-type semiconductor nature and high OER

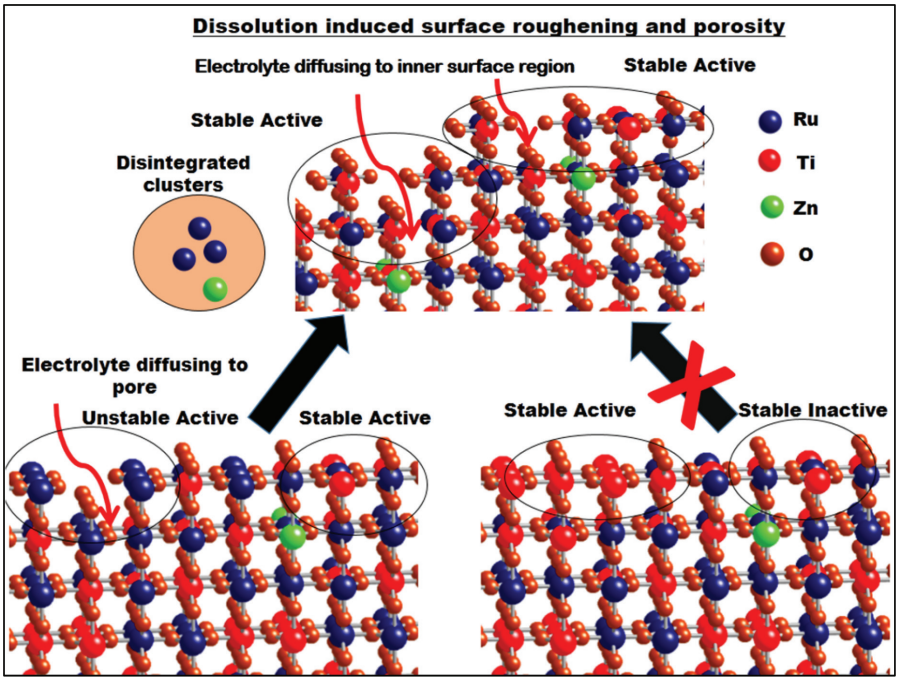

Figure 7: Enhanced porosity and surface roughening due to dissolution of unstable surface components (predominantly Ru and Zn) in Zn-doped RuO_2 – TiO_2 electrocatalyst. (110) surface has undergone dissolution to form kink, which has higher degree of under coordination.[61]

Table 3: Comparison of electrochemical OER activity of different electrocatalysts in acidic medium.

Electrocatalysts	Overpotential needed to reach 10 mA/cm² (mV) or * Activity at an overpotential of 350 mV (mA/cm²)	Tafel slope (mV/dec)	References
Crystalline RuO_2	450 mV (*7)	52	61
RuO_2 (110) thin film	#0.65	56	56
RuO_2 (100) thin film	#0.18	54	56
Amorphous RuO_2	220 mV (*42)	33	82
IrO_2	450 mV (*4.6)	58	55,105
IrO_2 (110) thin film	#0.0005	55	56
IrO_2 (100) thin film	#0.003	61	56
$Ru_{0.3}Ti_{0.7}$ (RuO_2-TiO_2)	*37	56	61
$Ru_{0.25}Ti_{0.74}Zn_{0.01}Ox$ (Zn-doped RuO_2-TiO_2)	*55	33	61
$Ru_{0.5}Ir_{0.5}$ (RuO_2–IrO_2)	—	58	55
IrO_2@RuO_2	250 mV	58	106
$Ru_{0.80}Ir_{0.15}Ce_{0.05}O_2$ (Ce-doped RuO_2-IrO_2)	—	46	95
$Mn_{0.76}Ti_{0.24}O_2$	^ 4	113	104

^ Activity at an overpotential of 600 mV (mA/cm²).
# Activity at an overpotential of 300 mV (mA/cm²).

activation barrier.[52] A TiO_2–MnO_2 electrocatalyst was found to show good stability and activity in acidic medium.[49,104] MnO_2 is stable only up to 1.6 V RHE and beyond this it starts to undergo dissolution. The dissolution front in doped-MnO_2 stops once it encounters Ti-surface atoms and the stability is retained for long duration. Also, Ti prefers to be under coordinated sites in MnO_2, hence additional synthetic treatment is not required for making the electrocatalyst stable.[49]

3.2 *OER electrocatalyst for alkaline electrolysis*

Though there are several challenges with alkaline water electrolyzer, lower cost coupled with the fact that there is greater material choice makes it a worthy option for extensive exploration. Unlike acidic medium, oxides of non-Noble elements (e.g., Ni, Co, Mn) are stable in alkaline medium over a higher range of anodic potential. The trend of activity among electrochemically prepared oxyhydroxide is Ni > Co > Fe[107] and monolayer thin-film oxyhydroxides also have similar activity order with Ni > Co > Fe > Mn.[108] However, computational studies indicate a different activity order Co > Ni > Mn.[48] Depending upon anodic potential, these metals undergo transformation from hydroxide to oxyhydroxide to oxide forms. In addition to their surface OER activity, the electronic properties and conductivity also widely vary due to the formation of different phases. This influences the overall OER activity and the activity trends among non-Noble oxides are found to be potential dependent.[109]

Cobalt-based electrocatalyst: Cobalt oxide is an important OER catalyst in alkaline medium and the literature has exclusive review on its behavior.[110,111] Co-electrocatalyst forms different forms of water oxidation catalysts such as Co_3O_4, CoOOH and $Co(OH)_2$. During OER, Co undergoes surface oxidation from Co(II) → Co(III) → Co(IV).[112,113] Also, surface reconstruction takes place depending upon electrochemical potential and electrochemical activity being proportional to the surface density of Co (III) sites. DFT studies indicate that CoOOH (1014) surface is the most stable below 1.13 V RHE, while CoOOH (0112) surface is predominantly above this potential.[114] In spinel oxide of Co_3O_4, Co (II) site remains inert, while Co (III) site is responsible for OER activity. This was proved by the fact that blocking Co (II) site by inert Zn atom does not hamper OER activity but blocking Co (III) site by inert Al atom significantly reduces it.[115]

Also, the OER activity is facet dependent and modulated synthesis procedure has to be employed to attain high active facets.[46,116–119] Another option is amorphization of the catalysis through (i) low temperature heating, or (ii) controlled electrochemical reduction.[120,121] Also, metal-organic framework decomposition-derived Co_3O_4 electrocatalysts show high activity due to their porous 3D configuration.[122–124]

Introduction of dopant in cobalt-based electrocatalyst can substantially increase its OER activity. DFT simulation studies predict that doping of Ni and V in Co-sites of (1014) and (0112) surfaces would lower the activation barrier of OER.[114] It has also been demonstrated experimentally that $NiCoO_2$ is five times better in terms of specific activity compared to Co_3O_4.[33]

Fe incorporation also increases the intrinsic activity of CoOOH ~100-fold, with peak activity for 40–60% Fe.[125] The Co films have Tafel slopes of ~62 mV/dec and Fe dopant between $0.33 < x < 0.79$ leads to Tafel slopes of 26–39 mV/dec. The stability will decrease with increase in Fe content. Incorporation of Fe dopant does not increase conductivity in CoOOH and after a certain Fe percentage, conductivity will even decrease. Fe dopant shifts the anodic peak of Co(II) → Co(III) compared to what occurs in Co-oxide/oxyhydroxide and makes oxidation of Co (II) more difficult. Fe provides the active sites instead of CoOOH and the energetics of OER for surface Fe sites in CoOOH is far more different than FeOOH. Among other dopants, Cu[126], Zn[127,128], Cr, Mn[129] increase the OER activity of co-oxides or their oxyhydroxide. However, the increase in activity does not appear significant in comparison to either Fe or Ni dopants.

Nickel-based electrocatalyst: Nickel oxide is among the other important electrocatalysts due to its high activity though its stability is an issue. Ni has several oxide, oxyhydroxide (β-NiOOH, γ-NiOOH) and hydroxide polymorphs [α-$Ni(OH)_2$, β-$Ni(OH)_2$].[107,130] Less crystalline α-$Ni(OH)_2$ polymorph gradually changes into a more crystalline β-$Ni(OH)_2$ phase during potential cycling in strong alkaline medium. It has also been suggested that the β-$Ni(OH)_2$ phase is the most active for OER since its oxidation to the β-NiOOH phase represents the optimal condition for the OER to occur.[107,131] However, during the initial electrochemical cycling, α-$Ni(OH)_2$ was found to be a better electrocatalyst than β-$Ni(OH)_2$.[132] Similarly, ordered β-NiOOH phase is generally formed during electrochemical cycling though disordered γ-NiOOH phase is more active for OER. The onset of OER is accompanied by Ni (II) → Ni (III) → Ni (IV) transformation.[133–135]

To improve electrocatalytic performance of Ni-based electrocatalyst, doped oxides are being made. Among the first-row transition metals, doping of Fe in NiO_x results in significant increase in its activity.[136–138] Even small amount of Fe doping results in significant increase in activity.[134] Incorporation of Fe dopant result leads to almost 30-fold enhancement of conductivity. Additionally, Fe incorporation leads to changes in electronic structure of NiOOH. Electrochemical studies show an anodic shift of the Ni redox waves with increasing Fe content in NiFeOOH indicating

lowering of Ni-oxidation states[139–142] contrary to claims of some researchers that Fe doping and associated partial charge transfer and formation of Ni (IV) are easier in NiOOH structure.[108,134,140] Computational studies with the support of experimental studies suggest that the Fe-O bond distance in Fe-doped NiOOH is unusually short, which is responsible for lowering of overall OER intermediates leading to the conclusion that Fe is the actual active site in NiFeOOH.[142,143] As like other electrocatalysts, morphology modulation towards higher aspect ratio nanostructures, generation of 3D microstructure of electrocatalyst[144,145] and amorphization of Fe-doped NiOOH leads to higher apparent electrocatalytic activity. The addition of other elements (e.g., Ce, Al, Co) may have additional effects, but does not appear to dramatically enhance OER activity.[138]

Iron-based electrocatalyst: Due to the abundance of Fe in earth's crust and nontoxicity, Fe-based electrocatalysts are appealing. The Fe-based oxide, oxyhydroxide, and hydroxides are less active, unstable and have low bulk conductivity.[65,107,108,146,147] Fundamental studies on pure Fe-based electrocatalyst are severely constrained by the following factors: (i) Pure Fe-oxides and hydroxides are prone to corrosion in alkaline medium, and the relationship between activity and dissolution is difficult to deconvolute,[30,33,109] (ii) Fe does not exhibit clear reversible redox waves in the experimentally accessible electrochemical window making it difficult to calculate ECSA through integrating redox waves, and (iii) the low electrical conductivity of bulk Fe-oxide/hydroxides leads to further lowering of activity.[148] Stabilization by using other dopants leads to increase in activity, however, poor conductivity is always a problem. However, Fe(III) is indeed the best electrocatalyst for OER.[109,148] It is better to dope Fe in other oxides/hydroxides or oxyhydroxide than doping other transition metals in Fe-based matrices.

Manganese-based electrocatalyst: Mn forms oxides with different oxidation states depending upon the electrochemical potential.[149] At lower oxidation potential (below 0.5 V RHE), Mn_3O_4 was observed and Mn_2O_3 formed above 0.85 V RHE. Near OER potentials, Mn(III) → Mn(IV) transformation occurs and MnO_2 was formed above ~1.4 V RHE potential. Above 1.7 V RHE, dissolution sets in with the formation of MnO_4^- species with solution colour changing to violet. The presence of di-m-oxo-bridged Mn ions in the layered structure results in a pronounced redox and charge capacity behaviour but a relatively large Tafel slope by developing a layered and 3D cross-linked MnOx catalyst structure.[150] In contrast, the 3D cross-linked structures with both mono- and di-m-oxo-bridged Mn ions present lower intrinsic OER activity but a smaller Tafel slope.

3.3 *Support design for electrocatalyst*

An ideal support should be: (i) stable under reaction conditions, (ii) provide low charge-

Table 4: Comparison of electrochemical OER activity of different electrocatalysts in acidic medium.

Electrocatalysts	Overpotential needed to reach 10 mA/cm^2 (mV) or * Activity at an overpotential of 350 mV (mA/cm^2)	Tafel slope (mV/dec)	References
CoO_x	600	42	136
Mesoporous Co_3O_4	290		124
NiO_x	472	30	136
$NiCoO_x$	400	33	136
α-$Ni(OH)_2$	331	42	132
$NiFeO_x$	336	30	151
NiFe-LDH	340	35	152
IrO_2	325		30
RuO_2	380	65	33
$LiNiO_2$	410	42	33
$LaNiO_3$	450	67	33
Mn_2O_3	530	69	33
α-MnO	490	78	153
δ-MnO_2	740	189	153
Mn_3O_4	430	60	33

transfer resistance, (iii) lower charge density around metal atoms of metal oxide electrocatalyst through electrocatalyst-support interactions, which in turn lowers the activation barrier for OER, and (iv) provide mechanical stability to the electrocatalysts, which are often in the form of nanostructures or thin films. It is generally agreed that among all the support materials Au performs best for thin film (< 5 monolayer) electrocatalysts since it is (i) the most electronegative metal and can increase the oxidation state of metal atom (e.g., Co, Mn, Ni) population on the surface by acting as an electron sink,[112120,154–156] (ii) it has high electrical conductivity, and (iii) is stable in OER conditions. However, it is prohibitively expensive, which restricts its utility in electrolyser. Also, taking account of 3D electrocatalyst, which may have a thickness of greater than >10 monolayer, the electronegativity effect of Au gets reduced.[112] This leads to search for alternative cost-effective supports, which can influence the electrocatalyst via (i) electronegativity that can cause changes in electronic structure, (ii) electrical conductivity that can reduce the charge-transfer resistance in the bulk, and (3) support faceting. The exposure of highly active facets due to support faceting is extremely case-specific in nature and is dependent on crystal-growth mechanism of electrocatalyst on the surface. During conformal thick film growth, the effect of support faceting is sometimes lost due to reorientation of stacking of planes and generation of polycrystalline films. However, activity of OER for thin film electrocatalyst is significantly affected due to support-faceting. This has been demonstrated by Switzer *et al*. by epitaxial growth of Co_3O_4 on Au and stainless steel support.[117] The morphology and XRD of the grown thin films have been found to be different for the same amount of electrocatalyst deposited.

To increase the OER activity, three-dimensional porous supports are also used. Highly porous carbon paper or zeolite support enables achieving high electrochemical surface area (ECSA).[157,158] However, low electrical conductivity of these support increases the charge-transfer resistance of electron transport thereby reducing the overall Faradaic efficiency of the OER support.[155,163] Furthermore, they have stability-related problems in higher potential regimes of OER. It is generally observed that OER rate increases at higher electrochemical potential, which would increase oxygen diffusion in the electrocatalyst and ultimately oxidizing the carbon support itself. To alleviate electrical conductivity-related problems, some researchers suggest using porous metallic framework such as Ni or Cu foam as a supporting material.[159]

Other approaches to increasing efficiency include making a metallic interlayer within the porous carbon paper itself, thereby providing an alternate low resistance path of electron transport. A recent study by Pala *et al.* showed that Cu would be the best metal among non-Noble transition metals for making interlayer in porous carbon support for increasing OER activity.[151] It is found that OER activity of the catalyst varies almost linearly with conductivity of the mellic interlayer (see Figure 8). When OER activity is plotted with the conductivity of metallic interlayer, two classes of behavior of metal supports are discernible: (i)

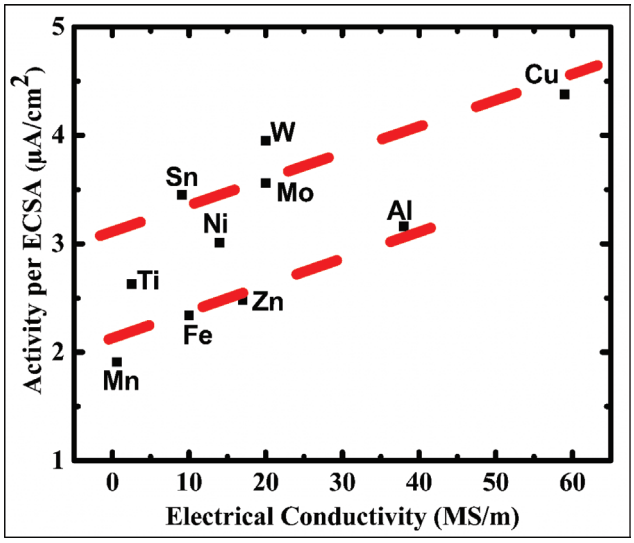

Figure 8: Specific activity (activity/ECSA) at an overpotential of 0.4 V (vs Ag/AgCl) vs conductivity of Co_3O_4 on metallic interlayer plot of different EAM-modified carbon supports.[151]

metals behaving like electron-sink give higher activity, and (ii) metals behaving like electron donor give lower activity. Supra- or sublinear behavior of the electrocatalyst was observed depending upon whether the metal is electron-sink or electron-donor. Correlations between OER activity with conductivity is especially important in the case of thick film three-dimensional electrocatalysts, while in the case of thin films, electronic interaction between support-electrocatalysts is more important as mentioned earlier.

The supports are broadly classified as: (i) porous three-dimensional, (3D) supports, which can provide high surface area (e.g., graphene, Ni foam, silica, zeolite),[117,159–166] and the porous structure of carbon or zeolite support enables achieving high electrochemical surface area (ECSA) for electrocatalysts resulting in higher activity though they have low electrical conductivity of carbon paper in comparison to metal support, which increases resistance for electron transport, thereby reducing overall efficiency.[123,165,167]

It is imperative to have strong interfacial bonding between electrocatalysts and support for stabilizing the electrode. However, lattice mismatch at interfaces make its formation difficult, which in turn reduces the stability of the electrode. One way to reduce the strain at electrode-support interface is to link electrocatalyst with support through conducting covalent linkage, e.g., click linkage of azide-alkyne.[168–173] Click-linked electrocatalysts and support show same degree of electrocatalytic activity in comparison to unclicked electrocatalysts due to conducting click-linkage with a higher degree of stability.

4 Electrolysers for Oxygen Evolution Reaction

4.1 *Electrolyser design*

An electrolyser comprises the following components: (i) cathode, (ii) anode, (iii) current collector, and (iv) ion-exchange membrane. Cathode, anode and ion-exchange of membrane are in conjugation known as gas-diffusion layer (GDL). The gas-diffusion layer and current collector are connected to make the whole membrane electrode assembly (MEA). Separator is used in between cathode and anode for both kinds of cells to avoid the mixing of oxygen and hydrogen produced during water electrolysis. Asbestos was commonly used as a separator but now it has been replaced with oxide ceramic materials or polysulfone. Generally, the gap between the electrodes is kept minimal for reducing the ohmic loss occurring in the electrolyte of the water electrolysis cell. To reduce the gaps, compressive pressures are applied

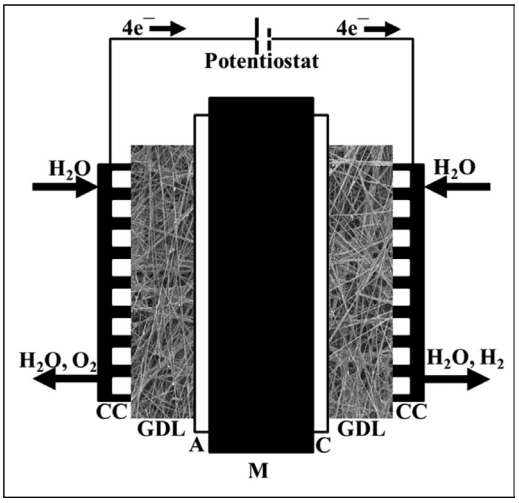

Figure 9: Polymer electrolyte membrane water electrolysis cell line diagram. Here in the figure, CC = current collector, GDL = gas diffusion layer, A = anode, C = cathode and M = ion exchange membrane. For producing the 1 m^3 hydrogen, PEM system generally consumes 3.8 kWh.

to make a compact electrolysis setup and lower contact resistance. Typically, high compressive pressure between gas diffusion layer (GDL) and current collector (CC) is applied through a nut-bolt assembly. The applied pressure reduces ohmic resistances offered by different components and interfaces of the cell (e.g., electrode-CC plate/bipolar plate interface), which are broadly termed as contact-resistance. However, the application of pressure affects the mesoporosity of the electrodes and reduces its expected electrocatalytic activity. This makes the design of pressurized electrolyzer more complicated and efforts are being made to rationalize some of the manufacturing techniques.[174]

4.1.1 Alkaline electrolysers: Alkaline electrolysers were first made available in 1975.[175] Earth-abundant electrocatalysts can be used in these types of electrolysers. They generally work at a temperature of 60–90°C. The electrode is typically synthesized by the nickel metal/metal oxide electrodeposited on metal plates. Alkaline electrolysis cells are available in two main categories, a filter press type and a tank type, which contain monopolar electrodes fitted in its tank. The filter press-type electrolyzer has complicated design in comparison to the type utilizing monopolar electrodes, and it uses bipolar electrodes, which are stacked together in several numbers. Lurgi-made filter press-type water electrolyzer can run at 32 bar. Newly developed alkaline water electrolyzer shows an overall efficiency of 80% and a current

efficiency 98% with 4–5 kWh electrical energy consumption. The purity of produced hydrogen and oxygen is higher than 99%.

4.1.2 Acidic electrolyzers: Acidic electrolyzers were developed by the General Electric Company back in 1950.[175] The liquid electrolyte was exchanged by the solid polymer electrolyte membranes like Nafion, which is a cation-conductive polymer membrane. An acidic water electrolyzer contains a stack of numerous MEA (membrane electrode assembly), which is separated by current collector diffusion layers that permit the produced gases and reactant water. The gas diffusion layer promotes optimal concentration of water and produced gases. The solid cation exchange membrane prevents the recombination of produced gases, oxygen and hydrogen. Acidic electrolyzers perform better in comparison to alkaline water electrolyzers with several advantages like achieving current density of 2 A/cm^2 at a comparatively lower power consumption.[175] The pressurized acidic electrolyzers can work under higher pressure with pressures up to 150 bar.[176]

5 Conclusion and Future Challenges

Water electrolysis to hydrogen and oxygen is one alternative way to balance fluctuating electricity generated through renewable energy sources such as solar, wind and tidal energy. To encourage clean energy generation and storage, both increase in efficiency and reduction in the cost of water electrolysers have to be accomplished. For this, the key challenge is to develop low-cost electrocatalysts, which can show low overpotential as well as low Tafel slope for both HER and OER. Though electrocatalysts for PEM electrolyzers show excellent performance for water splitting, they are generally made of Noble late transition elements, which increase the cost.

Various strategies have been considered for enhancing the performance of electrocatalysts either through increasing (i) specific activity, or (ii) active site density per geometrical surface area (GSA). Synthesis of mesoporous three-dimensional networks to increase surface area and active sites or exposing higher percentage of active facets through various morphologies has been explored. Employing multiple synthesis techniques, e.g., dealloying has been explored to increase the number of active sites in electrocatalysts. Even then, non-Noble electrocatalysts generally show lower activity and stability in comparison to Noble metal counterparts.

This leads to investigation of newer strategies to increase specific activities such as, (i) doping or alloying to get an active site distribution, which has Noble-metal-like properties or (ii) stabilization of non-native polymorphs of the material. In some cases, it has been observed that small changes to bond lengths/angles result in orders of magnitude differences in activity.[100,153,177–179] Doping leads to strain formation as well as change in d-band structure of host metal oxides, resulting in change in OER activity. Aliovalent doping leads to vacancy formation and it may produce additional effects like (i) bulk vacancies that increase the conductivity of the materials significantly leading to overall enhancement of OER activity due to reduced charge-transfer resistance, or (ii) surface vacancies leading to distorted metal octahedra configuration and to changes in energy barriers of reaction intermediates. The above reasons are thought to be valid for enhanced OER activity of Zn-doped RuO_2 and TiO_2.[61,98,100] Enhancing specific activity through polymorph engineering is still among less-investigated techniques. Kitchin *et al.* showed that coulombite IrO_2 would show 0.15 eV less activation barrier than rutile IrO_2.[180] The change in polymorphic structure results in huge change in d-band structure and considerable change in adsorption energies of intermediates. Also, it increases the possibility of stabilization of surfaces, which are structure-sensitive towards OER and thus can enhance the reaction rate considerably. One of the effective ways to stabilize these non-native polymorphs having low surface energy is through tuning surface to bulk ratio.[180] Also, certain supports preferentially stabilize specific non-native polymorphs in low-dimensional regime during epitaxial growth due to formation of coherent interfaces having favorable interfacial energy.[181,182] However, the stabilization of these metastable and non-native polymorphs still remains a challenge.

Although some progress has been made in obtaining low-cost electrocatalysts, which are both active and stable, some serious issues have not been resolved in relation to large-scale applications such as (i) large-scale synthesis, (ii) pressure-mediated loss of porosity in electrolysers, or (iii) inherent conductivity-related issues. Electrocatalysts should show excellent electrochemical stability, and have to be mechanically durable for many years so that the maintenance of electrolyzer does not create a problem. Furthermore, coating the electrocatalysts on the support should create a proper conductive interface to facilitate charge-transfer. This has been a problem for especially integrating solution-synthesized electrocatalysts

onto support for large-area electrodes. In addition, electrodes having carbon supports (CNTs, graphene) and some three-dimensional microstructures (core–shell nanostructures) with excellent electrocatalytic performances often show unsatisfactory mechanical stability. Therefore, the process of scaling up of electrocatalysts from lab-scale to industrial scale has to be addressed.

Furthermore, the electrochemical corrosion of the electrodes has to be addressed. Even non-precious pure metallic catalysts and many alloys suffer acidic corrosion for HER in acid solution. Corrosion problem is more severe for OER. At high anodic potentials for thin film electrodes, both the electrocatalyst and support show higher oxidation states. Furthermore, some of the metal oxide supports may show excellent stability but their conductivity is a big issue. Thus, finding electrochemically corrosion resistant and conductive OER electrocatalysts as well as their support is an urgent issue.

To be viable in the industrial front, the water electrolysers work at generally high current densities, such as 1–2 A/cm^2. The Department of Energy (DOE) of the United States has set a target for water electrolysis to operate at 2 A cm^{-2} with a cell potential of 1.5 V vs RHE by 2017.[183] However, the lab-scale benchmarking conditions for OER electrocatalysts are 10–100 mA/cm.^{2} This makes them viable only for low-current devices or where hydrogen demand is less. On the other hand, it should be noted that high-current conditions require different electroanalytical techniques beyond cyclic voltammetry or Tafel measurement, since they involve mass-transport limitations. Moreover, during the measurements, the generated oxygen could diffuse into the cathode chamber where it can be reduced to water on reaction with hydrogen. These phenomena would be significant when dealing with high current densities. In addition, the low current density achieved is also due to the high ohmic resistance offered by the liquid electrolyte and membrane. This supports the fact that there are additional components in addition to better electrocatalyst synthesis, which have to be looked into to increase the performance of electrolysers.

Better design of electrolysers would only be possible with increased understanding of several phenomena that occur during water electrolysis, e.g., (i) OER pathway under different electrochemical potential, (ii) charge transfer between electrocatalysts and support and electrode-electrolyte interface, (iii) corrosion reaction pathway and corrosion fronts during OER, (iv) electronic nature of active sites, and (v) diffusion of oxygen through electrolyte during electrolysis. Understanding of all these phenomena at basic atomistic level would help us to design better electrocatalysts, which would enable efficient cost-effective electrolysers.

Acknowledgment

We thank the Indian Space Research Organization (ISRO) and the Technology Systems Development program of the Department of Science and Technology for supporting this work.

Received 6 September 2016.

References

1. H. Abe, J. Liu and K. Ariga, Catalytic nanoarchitectonics for environmentally compatible energy generation, *Mater. Today*, **19**(1), 12–18 (2016).
2. J. Vatamanu and D. Bedrov, Capacitive Energy Storage: Current and Future Challenges, *J. Phys. Chem. Lett.*, **6**(18), 3594–3609 (2015).
3. P.C.K. Vesborg and T.F. Jaramillo, Addressing the terawatt challenge: scalability in the supply of chemical elements for renewable energy, *RSC Adv.*, **2**(21), 7933–7947 (2012).
4. M.I. Hoffert, K. Caldeira, G. Benford, D.R. Criswell, C. Green, H. Herzog, A.K. Jain, H.S. Kheshgi, K.S. Lackner and J.S. Lewis, Advanced technology paths to global climate stability: energy for a greenhouse planet, *Science*, **298**(5595), 981–987 (2002).
5. M. Balat, Potential importance of hydrogen as a future solution to environmental and transportation problems, *Int. J. Hydrogen Energ.*, **33**(15), 4013–4029 (2008).
6. N. Armaroli and V. Balzani, The future of energy supply: challenges and opportunities, *Angew. Chem.*, **46**(1), 52–66 (2007).
7. S. Chu and A. Majumdar, Opportunities and challenges for a sustainable energy future, *Nature*, **488**(7411), 294–303 (2012).
8. R. Ramachandran and R.K. Menon, An overview of industrial uses of hydrogen, *Int. J. Hydrogen Energ.*, **23**(7), 593–598 (1998).
9. R. Kothari, D. Buddhi and R.L. Sawhney, Comparison of environmental and economic aspects of various hydrogen production methods, *Renewable Sustainable Energ. Rev.*, **12**(2), 553–563 (2008).
10. S.G. Chalk, J.F. Miller, Key challenges and recent progress in batteries, fuel cells and hydrogen storage for clean energy systems, *J. Power Sources*, **159**(1), 73–80 (2006).
11. M.T. Balta, O. Kizilkan and F. Yılmaz, Energy and exergy analyses of integrated hydrogen production system using high temperature steam electrolysis, *Int. J. Hydrogen Energ.*, **41**(19), 8032–8041 (2016).
12. A.G. Dutton, J.A.M. Bleijs, H. Dienhart, M. Falchetta, W. Hug, D. Prischich, A.J. Ruddell, Experience in the design, sizing, economics and implementation of autonomous

wind-powered hydrogen production systems, *Int. J. Hydrogen Energ.*, **25**(8), 705–722 (2000).
13. F.F. Abdi, L. Han, A.H. Smets, M. Zeman, B. Dam and R. van de Krol, Efficient solar water splitting by enhanced charge separation in a bismuth vanadate-silicon tandem photoelectrode, *Nat. Comm.*, **4**(2195), 1–7 (2013).
14. O. Khaselev and J.A. Turner, A Monolithic Photovoltaic-Photoelectrochemical Device for Hydrogen Production via Water Splitting, *Science*, **280**(5362), 425–427 (1998).
15. C. Yilmaz and M. Kanoglu, Thermodynamic evaluation of geothermal energy powered hydrogen production by PEM water electrolysis, *Energy*, **69**, 592–602 (2014).
16. M. Grätzel, Photoelectrochemical cells, *Nature*, **414**(6861), 338–344 (2001).
17. M.G. Walter, E.L. Warren, J.R. McKone, S.W. Boettcher, Q. Mi, E.A. Santori and N.S. Lewis, Solar water splitting cells, *Chem. Rev.*, **110**(11), 6446–6473 (2010).
18. K. Zeng and D. Zhang, Recent progress in alkaline water electrolysis for hydrogen production and applications, *Prog. in Energ. Combustion Sci.*, **36**(3), 307–326 (2010).
19. F. Barbir, PEM electrolysis for production of hydrogen from renewable energy sources, *Solar Energ.*, **78**(5), 661–669 (2005).
20. K. Zeng and D. Zhang, Recent progress in alkaline water electrolysis for hydrogen production and applications, *Prog. Energ. Combust. Sci.*, **36**(3), 307–326 (2010).
21. H.B. Beer, The invention and industrial development of metal anodes, *J. Electrochem. Soc.*, **127**(8), 303C-307C (1980).
22. M.A. Hickner, A.M. Herring and E.B. Coughlin, Anion exchange membranes: current status and moving forward, *J. Polymer Sci. Part B: Polymer Phys*, **51**(24), 1727–1735 (2013).
23. R. Marcus, On the theory of oxidation—reduction reactions involving electron transfer. v. comparison and properties of electrochemical and chemical rate constants[1], *J. Phys. Chem.*, **67**(4), 853–857 (1963).
24. J.-M. Saveant and D. Tessier, Variation of the electrochemical transfer coefficient with potential, *Faraday Discuss. Chem. Soc.*, **74**(0), 57–72 (1982).
25. R. Marcus, Exchange reactions and electron transfer reactions including isotopic exchange. Theory of oxidation-reduction reactions involving electron transfer. Part 4.—A statistical-mechanical basis for treating contributions from solvent, ligands and and inert salt, Discuss, *Faraday Soc.*, **29**, 21–31 (1960).
26. Z. Yang, J. Zhang, M.C.W. Kintner-Meyer, X. Lu, D. Choi, J.P. Lemmon and J. Liu, Electrochemical energy storage for green grid, *Chem. Rev.*, **111**(5), 3577–3613 (2011).
27. F.T. Wagner, B. Lakshmanan and M.F. Mathias, Electrochemistry and the future of the automobile, *J. Phys. Chem. Lett*, **1**(14), 2204–2219.
28. E. Barendrecht, Electrochemistry of fuel cells, in: Fuel cell systems, Springer, (1993), pp. 73–119.
29. C.C.L. McCrory, S. Jung, I.M. Ferrer, S. Chatman, J.C. Peters and T.F. Jaramillo, Benchmarking HER and OER Electrocatalysts for Solar Water Splitting Devices, *J. Am. Chem. Soc.*, **137**(13), 4347–4357 (2015).
30. C.C.L. McCrory, S. Jung, J.C. Peters and T.F. Jaramillo, Benchmarking Heterogeneous Electrocatalysts for the Oxygen Evolution Reaction, *J. Am. Chem. Soc.*, **135**(45), 16977–16987 (2013).
31. A. Pozio, M. De Francesco, A. Cemmi, F. Cardellini and L. Giorgi, Comparison of high surface Pt/C catalysts by cyclic voltammetry, *J. Power Sources*, **105**(1), 13–19 (2002).
32. H.A. Gasteiger, N. Markovic, P.N. Ross Jr and E.J. Cairns, Carbon monoxide electrooxidation on well-characterized platinum-ruthenium alloys, *J. Phys. Chem.*, **98**(2), 617–625 (1994).
33. S. Jung, C.C.L. McCrory, I.M. Ferrer, J.C. Peters and T.F. Jaramillo, Benchmarking nanoparticulate metal oxide electrocatalysts for the alkaline water oxidation reaction, *J. Mater. Chem. A*, **4**(8), 3068–3076 (2016).
34. Y. Matsumoto and E. Sato, Electrocatalytic properties of transition metal oxides for oxygen evolution reaction, *Mater. Chem. Phys.*, **14**(5), 397–426 (1986).
35. A. Vojvodic and J.K. Nørskov, Optimizing perovskites for the water-splitting reaction, *Science*, **334**(6061), 1355–1356 (2011).
36. S. Trasatti and O. Petrii, Real surface area measurements in electrochemistry, *J. Electroanal. Chem.*, **327**(1–2), 353–376 (1992).
37. G. Prentice, Electrochemical engineering principles, pp. 95–96, Prentice Hall (1991).
38. J. Tymoczko, W. Schuhmann and A.S. Bandarenka, The constant phase element reveals 2D phase transitions in adsorbate layers at the electrode/electrolyte interfaces, *Electrochem. Comm.*, **27**, 42–45 (2013).
39. Z. Kerner and T. Pajkossy, On the origin of capacitance dispersion of rough electrodes, *Electrochim. Acta*, **46**(2–3), 207–211 (2000).
40. S.K. Roy and M.E. Orazem, Graphical estimation of interfacial capacitance of PEM fuel cells from impedance measurements, *J. Electrochem. Soc.*, **156**(2), B203–B209 (2009).
41. I. Katsounaros, J.C. Meier and K.J. Mayrhofer, The impact of chloride ions and the catalyst loading on the reduction of H_2O_2 on high-surface-area platinum catalysts, *Electrochim. Acta*, **110**, 790–795 (2013).
42. J.K. Nørskov, J. Rossmeisl, A. Logadottir, L. Lindqvist, J.R. Kitchin, T. Bligaard and H. Jonsson, Origin of the overpotential for oxygen reduction at a fuel-cell cathode, *J. Phys. Chem*. B, **108**(46), 17886–17892 (2004).
43. L. Zhang and Z. Xia, Mechanisms of oxygen reduction reaction on nitrogen-doped graphene for fuel cells, *J. Phys. Chem*. C, **115**(22), 11170–11176 (2011).
44. E. Skúlason, G.S. Karlberg, J. Rossmeisl, T. Bligaard, J. Greeley, H. Jónsson and J.K. Nørskov, Density functional theory calculations for the hydrogen evolution reaction in an electrochemical double layer on the Pt (111) electrode, *Phys. Chem. Chem. Phys.*, **9**(25), 3241–3250 (2007).

45. R.G.S. Pala, W. Tang, M.M. Sushchikh, J.-N. Park, A.J. Forman, G. Wu, A. Kleiman-Shwarsctein, J. Zhang, E.W. McFarland and H. Metiu, CO oxidation by Ti- and Al-doped ZnO: oxygen activation by adsorption on the dopant, *J. Catal.*, **266**(1), 50–58 (2009).
46. C.P. Plaisance, R.A. van Santen and Structure Sensitivity of the Oxygen Evolution Reaction Catalyzed by Cobalt (II, III) Oxide, *J. Am. Chem. Soc.*, **137**(46), 14660–14672 (2016).
47. M. Garcia-Mota, A. Vojvodic, F. Abild-Pedersen and J.K. Norskov, Electronic Origin of the Surface Reactivity of Transition-Metal-Doped TiO_2(110), *J. Phys. Chem. C*, **117**(1), 460–465 (2013).
48. I.C. Man, H.-Y. Su, F. Calle-Vallejo, H.A. Hansen, J.I. Martínez, N.G. Inoglu, J. Kitchin, T.F. Jaramillo, J.K. Norskov and J. Rossmeisl, Universality in Oxygen Evolution Electrocatalysis on Oxide Surfaces, *Chem Cat Chem*, **3**(7), 1159–1165 (2011).
49. R. Frydendal, E.A. Paoli, I. Chorkendorff, J. Rossmeisl and I.E. Stephens, Toward an Active and Stable Catalyst for Oxygen Evolution in Acidic Media: Ti-Stabilized MnO_2, *Adv. Energ. Mater.*, **5**(22), (2015).
50. J.M. Bockris, Kinetics of activation controlled consecutive electrochemical reactions: anodic evolution of oxygen, *J. Chem. Phys.*, **24**(4), 817(1956).
51. M. Wohlfahrt-Mehrens and J. Heitbaum, Oxygen evolution on Ru and RuO_2 electrodes studied using isotope labelling and on-line mass spectrometry, *J. Electroanal. Chem. Interfac. Electrochem.*, **237**(2), 251–260 (1987).
52. J. Rossmeisl, Z.W. Qu, H. Zhu, G.J. Kroes and J.K. Norskov, Electrolysis of water on oxide surfaces, *J. Electroanal. Chem.*, **607**(1–2), 83–89 (2007).
53. Y.-H. Fang and Z.-P. Liu, Mechanism and tafel lines of electro-oxidation of water to oxygen on RuO_2 (110), *J. Am. Chem. Soc.*, **132**(51), 18214 (2010).
54. P. Castelli, S. Trasatti, F.H. Pollak and W.E. O'Grady, Single crystals as model electrocatalysts, *J. Electroanal. Chem. Interfac. Electrochem.*, **210**(1), 189–194 (1986).
55. M.E.G. Lyons and S. Floquet, Mechanism of oxygen reactions at porous oxide electrodes. Part 2: Oxygen evolution at RuO_2, IrO_2 and $IrxRu_1$-xO_2 electrodes in aqueous acid and alkaline solution, *Phys. Chem. Chem. Phys.*, **13**(12), 5314–5335 (2011).
56. K.A. Stoerzinger, L. Qiao, M.D. Biegalski and Y. Shao-Horn, Orientation-Dependent Oxygen Evolution Activities of Rutile IrO_2 and RuO_2, *J. Phys. Chem. Lett.*, **5**(10), 1636–1641 (2014).
57. T. Binninger, R. Mohamed, K. Waltar, E. Fabbri, P. Levecque, R. Kötz and T.J. Schmidt, Thermodynamic explanation of the universal correlation between oxygen evolution activity and corrosion of oxide catalysts, *Sci. Rep.*, **5**(2015).
58. N. Danilovic, R. Subbaraman, K.-C. Chang, S.H. Chang, Y.J. Kang, J. Snyder, A.P. Paulikas, D. Strmcnik, Y.-T. Kim, D. Myers, V.R. Stamenkovic and N.M. Markovic, Activity–Stability Trends for the Oxygen Evolution Reaction on Monometallic Oxides in Acidic Environments, *J. Phys. Chem. Lett.*, **5**(14), 2474–2478 (2014).
59. R. Kötz, H. Neff and S. Stucki, Anodic Iridium Oxide Films XPS-Studies of Oxidation State Changes and O_2 evolution, *J. Electrochem. Soc.*, **131**(1), 72–77 (1984).
60. R. Kotz, H.J. Lewerenz and S. Stucki, XPS studies of oxygen evolution on Ru and RuO_2 anodes, *J. Electrochem. Soc.*, **130**(4), 825–829 (1983).
61. K. Kishor, S. Saha, M.K. Gupta, A. Bajpai, M. Chatterjee, S. Sivakumar and R.G.S. Pala, Roughened Zn-Doped Ru–Ti Oxide Water Oxidation Electrocatalysts by Blending Active and Activated Passive Components, *Chem Electro Chem*, **2**(11), 1839–1846 (2015).
62. A.J. Medford, A. Vojvodic, J.S. Hummelshøj, J. Voss, F. Abild-Pedersen, F. Studt, T. Bligaard, A. Nilsson and J.K. Nørskov, From the Sabatier principle to a predictive theory of transition-metal heterogeneous catalysis, *J. Catal.*, **328**, 36–42 (2015).
63. R.G.S. Pala, Computer-aided design of doped oxide catalysts, *J. Ind. Inst. Sci.*, **90**(2), 163–180 (2012).
64. S. Trasatti, Electrocatalysis by oxides—Attempt at a unifying approach, *J. Electroanal. Chem. Interfac. Electrochem.*, **111**(1), 125–131 (1980).
65. S. Trasatti, Electrocatalysis in the anodic evolution of oxygen and chlorine, *Electrochim. Acta*, **29**(11), 1503–1512 (1984).
66. S. Trasatti, Physical electrochemistry of ceramic oxides, *Electrochim. Acta*, **36**(2), 225–241 (1991).
67. N.B. Halck, V. Petrykin, P. Krtil and J. Rossmeisl, Beyond the volcano limitations in electrocatalysis—oxygen evolution reaction, *Phys. Chem. Chem. Phys.*, **16**(27), 13682–13688 (2014).
68. M. Busch, N.B. Halck, U.I. Kramm, S. Siahrostami, P. Krtil and J. Rossmeisl, Beyond the top of the volcano?—A unified approach to electrocatalytic oxygen reduction and oxygen evolution, Nano Energy, (Just Accepted), (2016).
69. C.K. Rastogi, S. Saha, S. Sivakumar, R.G.S. Pala and J. Kumar, Kinetically stabilized aliovalent europium-doped magnesium oxide as a UV sensitized phosphor, *Phys. Chem. Chem. Phys.*, **17**(6), 4600–4608 (2015).
70. J. Rossmeisl, A. Logadottir and J.K. Norskov, Electrolysis of water on (oxidized) metal surfaces, *Chem. Phys.*, **319**(1), 178–184 (2005).
71. M.M. Montemore and J.W. Medlin, Scaling relations between adsorption energies for computational screening and design of catalysts, *Catal. Sci. Tech.*, **4**(11), 3748–3761 (2014).
72. A. Vojvodic, A. Hellman, C. Ruberto and B.I. Lundqvist, From electronic structure to catalytic activity: A single descriptor for adsorption and reactivity on transition-metal carbides, *Phys. Rev. Lett.*, **103**(14), 146103 (2009).
73. F. Lima, J. Zhang, M. Shao, K. Sasaki, M. Vukmirovic, E. Ticianelli and R. Adzic, Catalytic activity-d-band center correlation for the O_2 reduction reaction on platinum in alkaline solutions, *J. Phys. Chem. C*, **111**(1), 404–410 (2007).

74. B. Hammer and J. Norskov, Why gold is the noblest of all the metals, *Nature*, **376**(6537), 238–240 (1995).
75. J. Suntivich, K.J. May, H.A. Gasteiger, J.B. Goodenough and Y. Shao-Horn, A perovskite oxide optimized for oxygen evolution catalysis from molecular orbital principles, *Science*, **334**(6061), 1383–1385 (2011).
76. A. Grimaud, K.J. May, C.E. Carlton, Y.-L. Lee, M. Risch, W.T. Hong, J. Zhou and Y. Shao-Horn, Double perovskites as a family of highly active catalysts for oxygen evolution in alkaline solution, *Nat. Comm.*, **4**(2013).
77. Z. Xu and J.R. Kitchin, Relationships between the surface electronic and chemical properties of doped 4d and 5d late transition metal dioxides, *J. Chem. Phys.*, **142**(10), 104703 (2015).
78. F. Calle-Vallejo, N.G. Inoglu, H.-Y. Su, J.I. Martinez, I.C. Man, M.T.M. Koper, J.R. Kitchin and J. Rossmeisl, Number of outer electrons as descriptor for adsorption processes on transition metals and their oxides, *Chem. Sci.*, **4**(3), 1245–1249 (2013).
79. S. Cherevko, A.R. Zeradjanin, A.A. Topalov, N. Kulyk, I. Katsounaros and K.J. Mayrhofer, Dissolution of noble metals during oxygen evolution in acidic media, *Chem Cat Chem*, **6**(8), 2219–2223 (2014).
80. M. Miles and M. Thomason, Periodic variations of overvoltages for water electrolysis in acid solutions from cyclic voltammetric studies, *J. Electrochem. Soc.*, **123**(10), 1459–1461 (1976).
81. H. Ma, C. Liu, J. Liao, Y. Su, X. Xue and W. Xing, Study of ruthenium oxide catalyst for electrocatalytic performance in oxygen evolution, *J. Mol. Catal. A: Chem.*, **247**(1–2), 7–13 (2006).
82. E. Tsuji, A. Imanishi, K.-i. Fukui and Y. Nakato, Electrocatalytic activity of amorphous RuO_2 electrode for oxygen evolution in an aqueous solution, *Electrochim. Acta*, **56**(5), 2009–2016 (2011).
83. N. Hodnik, P. Jovanovič, A. Pavlišič, B. Jozinovič, M. Zorko, M. Bele, V.S. Šelih, M. Šala, S. Hočevar and M. Gaberšček, New Insights into Corrosion of Ruthenium and Ruthenium Oxide Nanoparticles in Acidic Media, *J. Phys. Chem. C*, **119**(18), 10140–10147 (2015).
84. E.A. Paoli, F. Masini, R. Frydendal, D. Deiana, C. Schlaup, M. Malizia, T.W. Hansen, S. Horch, I.E. Stephens and I. Chorkendorff, Oxygen evolution on well-characterized mass-selected Ru and RuO_2 nanoparticles, *Chem. Sci.*, **6**(1), 190–196 (2015).
85. T. Reier, M. Oezaslan, P. Strasser, Electrocatalytic Oxygen Evolution Reaction (OER) on Ru and Ir, and Pt Catalysts: A Comparative Study of Nanoparticles and Bulk Materials, *ACS Catal.*, **2**(8), 1765–1772 (2012).
86. B. Johnson, F. Girgsdies, G. Weinberg, D. Rosenthal, A. Knop-Gericke, R. Schlögl, T. Reier and P. Strasser, Suitability of Simplified (Ir,Ti)Ox Films for Characterization during Electrocatalytic Oxygen Evolution Reaction, *J. Phys. Chem. C*, **117**(48), 25443–25450 (2013).
87. S. Cherevko, T. Reier, A.R. Zeradjanin, Z. Pawolek, P. Strasser and K.J. Mayrhofer, Stability of nanostructured iridium oxide electrocatalysts during oxygen evolution reaction in acidic environment, *Electrochem. Comm.*, **48**, 81–85 (2014).
88. H.-S. Oh, H.N. Nong, T. Reier, M. Gliech and P. Strasser, Oxide-supported Ir nanodendrites with high activity and durability for the oxygen evolution reaction in acid PEM water electrolyzers, *Chem. Sci.*, **6**(6), 3321–3328 (2015).
89. R. Kötz, H. Neff and S. Stucki, Anodic Iridium Oxide Films XPS-Studies of Oxidation State Changes and O_2-Evolution, *J. Electrochem. Soc.*, **131**(1), 72–77 (1984).
90. S. Hackwood, L. Schiavone, W. Dautremont-Smith and G. Beni, Anodic evolution of oxygen on sputtered iridium oxide films, *J. Electrochem. Soc.*, **128**(12), 2569–2573 (1981).
91. X. Wu and K. Scott, RuO_2 supported on Sb-doped SnO_2 nanoparticles for polymer electrolyte membrane water electrolysers, *Int. J. Hydrogen Energ.*, **36**(10), 5806–5810 (2011).
92. L.-A. Naslund, C.M. Sanchez-Sanchez, A.S. Ingason, J. Backstrom, E. Herrero, J. Rosen and S. Holmin, The Role of TiO_2 Doping on RuO_2-Coated Electrodes for the Water Oxidation Reaction, *J. Phys. Chem. C*, **117**(12), 6126–6135 (2013).
93. N. Danilovic, R. Subbaraman, K.C. Chang, S.H. Chang, Y. Kang, J. Snyder, A.P. Paulikas, D. Strmcnik, Y.T. Kim and D. Myers, Using Surface Segregation to Design Stable Ru-Ir Oxides for the Oxygen Evolution Reaction in Acidic Environments, *Angew. Chem.*, **126**(51), 14240–14245 (2014).
94. K. Kadakia, M.K. Datta, O.I. Velikokhatnyi, P. Jampani, S.K. Park, S.J. Chung, P.N. Kumta and High performance fluorine doped (Sn, Ru)O_2 oxygen evolution reaction electro-catalysts for proton exchange membrane based water electrolysis, *J. Power Sources*, **245**, 362–370 (2014).
95. T. Audichon, S. Morisset, T.W. Napporn, K.B. Kokoh, C. Comminges and C. Morais, Effect of Adding CeO_2 to RuO_2-IrO_2 Mixed Nanocatalysts: Activity towards the Oxygen Evolution Reaction and Stability in Acidic Media, *Chem Electro Chem*, **2**(8), 1128–1137 (2015).
96. M. García-Mota, A. Vojvodic, H. Metiu, I.C. Man, H.-Y. Su, J. Rossmeisl and J.K. Nørskov, Tailoring the Activity for Oxygen Evolution Electrocatalysis on Rutile TiO_2(110) by Transition-Metal Substitution, *Chem Cat Chem*, **3**(10), 1607–1611 (2011).
97. R.K. Karlsson, H.A. Hansen, T. Bligaard, A. Cornell and L.G. Pettersson, Ti atoms in $Ru_{0.3}Ti_{0.7}O_2$ mixed oxides form active and selective sites for electrochemical chlorine evolution, *Electrochim. Acta*, **146**, 733–740 (2014).
98. V. Petrykin, K. Macounova, J. Franc, O. Shlyakhtin, M. Klementova, S. Mukerjee and P. Krtil, Zn-Doped RuO_2 electrocatalyts for Selective Oxygen Evolution: Relationship between Local Structure and Electrocatalytic Behavior in Chloride Containing Media, *Chem. Mater.*, **23**(2), 200–207 (2010).
99. V. Petrykin, K. Macounov, M. Okube, S. Mukerjee and P. Krtil, Local structure of Co doped RuO_2 nanocrystalline

electrocatalytic materials for chlorine and oxygen evolution, *Catal. Today*, **202**(0), 63–69 (2012).

100. V. Petrykin, K. Macounova, O.A. Shlyakhtin and P. Krtil, Tailoring the Selectivity for Electrocatalytic Oxygen Evolution on Ruthenium Oxides by Zinc Substitution, *Angew. Chem.*, **49**(28), 4813–4815 (2010).
101. V. Petrykin, Z. Bastl, J. Franc, K. Macounova, M. Makarova, S. Mukerjee, N. Ramaswamy, I. Spirovova and P. Krtil, Local Structure of Nanocrystalline Ru_1-x Ni xO_2-d Dioxide and Its Implications for Electrocatalytic Behavior-An XPS and XAS Study, *J. Phys. Chem. C*, **113**(52), 21657–21666 (2009).
102. D.K. Behara, A.K. Ummireddi, V. Aragonda, P.K. Gupta, R.G.S. Pala and S. Sivakumar, Coupled optical absorption, charge carrier separation and surface electrochemistry in surface disordered/hydrogenated TiO_2 for enhanced PEC water splitting reaction, *Phys. Chem. Chem. Phys.*, **18**(12), 8364–8377 (2016).
103. D.K. Behara, A.P. Upadhyay, G.P. Sharma, B. Kiran, S. Sivakumar and R.G.S. Pala, Heterostructures Based on TiO_2 and Silicon for Solar Hydrogen Generation, *Adv. Func. Mater.*, 219–281 (2015).
104. K.L. Pickrahn, A. Garg and S.F. Bent, ALD of Ultrathin Ternary Oxide Electrocatalysts for Water Splitting, *ACS Catal.*, **5**(3), 1609–1616 (2015).
105. Y. Lee, J. Suntivich, K.J. May, E.E. Perry and Y. Shao-Horn, Synthesis and Activities of Rutile IrO_2 and RuO_2 Nanoparticles for Oxygen Evolution in Acid and Alkaline Solutions, *J. Phys. Chem. Lett.*, **3**(3), 399–404 (2012).
106. T. Audichon, T.W. Napporn, C. Canaff, C. Morais, C. Comminges and K.B. Kokoh, IrO_2 Coated on RuO_2 as Efficient and Stable Electroactive Nanocatalysts for Electrochemical Water Splitting, *J. Phys. Chem. C*, **120**(5), 2562–2573 (2016).
107. M.E.G. Lyons, M.P. Brandon and A comparative study of the oxygen evolution reaction on oxidised nickel, cobalt and iron electrodes in base, *J. Electroanal. Chem.*, **641**(1), 119–130 (2010).
108. R. Subbaraman, D. Tripkovic, K.-C. Chang, D. Strmcnik, A.P. Paulikas, P. Hirunsit, M. Chan, J. Greeley, V. Stamenkovic, N.M. Markovic, Trends in activity for the water electrolyser reactions on 3d M (Ni, Co and Fe, Mn) hydr (oxy) oxide catalysts, *Nat. Mater.*, **11**(6), 550–557 (2012).
109. M.S. Burke, S. Zou, L.J. Enman, J.E. Kellon, C.A. Gabor, E. Pledger and S.W. Boettcher, Revised oxygen evolution reaction activity trends for first-row transition-metal (oxy) hydroxides in alkaline media, *J. Phys. Chem. Lett.*, **6**(18), 3737–3742 (2015).
110. X. Deng and H. Tuysuz, Cobalt-Oxide-Based Materials as Water Oxidation Catalyst: Recent Progress and Challenges, *ACS Catal.*, **4**(10), 3701–3714 (2014).
111. J. Wang, W. Cui, Q. Liu, Z. Xing, A.M. Asiri and X. Sun, Recent Progress in Cobalt-Based Heterogeneous Catalysts for Electrochemical Water Splitting, *Adv. Mater.*, **28**(2), 215–230 (2016).
112. B.S. Yeo and A.T. Bell, Enhanced Activity of Gold-Supported Cobalt Oxide for the Electrochemical Evolution of Oxygen, *J. Am. Chem. Soc.*, **133**(14), 5587–5593 (2011).
113. N. Weidler, S. Paulus, J. Schuch, J. Klett, S. Hoch, P. Stenner, A. Maljusch, J. Brötz, C. Wittich and B. Kaiser, CoO_x thin film deposited by CVD as efficient water oxidation catalyst: change of oxidation state in XPS and its correlation to electrochemical activity, *Phys. Chem. Chem. Phys.*, **18**(16), 10708–10718 (2016).
114. M. Bajdich, M. Garcia-Mota, A. Vojvodic, J.K. Norskov and A.T. Bell, Theoretical Investigation of the Activity of Cobalt Oxides for the Electrochemical Oxidation of Water, *J. Am. Chem. Soc.*, **135**(36), 13521–13530 (2013).
115. H.-Y. Wang, S.-F. Hung, H.-Y. Chen, T.-S. Chan, H.M. Chen and B. Liu, In Operando Identification of Geometrical-Site-Dependent Water Oxidation Activity of Spinel Co_3O_4, *J. Am. Chem. Soc.*, **138**(1), 36–39 (2016).
116. Z. Chen, C.X. Kronawitter and B.E. Koel, Facet-dependent activity and stability of Co_3O_4 nanocrystals towards the oxygen evolution reaction, *Phys. Chem. Chem. Phys.*, **17**(43), 29387–29393 (2015).
117. J.A. Koza, Z. He, A.S. Miller and J.A. Switzer, Electrodeposition of Crystalline Co_3O_4—A Catalyst for the Oxygen Evolution Reaction, *Chem. Mater.*, **24**(18), 3567–3573 (2012).
118. J.A. Koza, C.M. Hull, Y.-C. Liu and J.A. Switzer, Deposition of b-$Co(OH)_2$ Films by Electrochemical Reduction of Tris(ethylenediamine)cobalt(III) in Alkaline Solution, *Chem. Mater.*, **25**(9), 1922–1926 (2013).
119. Y.-C. Liu, J.A. Koza, J.A. Switzer and Conversion of electrodeposited $Co(OH)_2$ to CoOOH and Co_3O_4, and comparison of their catalytic activity for the oxygen evolution reaction, *Electrochim. Acta*, **140**, 359–365 (2014).
120. M.A. Sayeed, T. Herd and A.P. O'Mullane, Direct electrochemical formation of nanostructured amorphous $Co(OH)_2$ on gold electrodes with enhanced activity for the oxygen evolution reaction, *J. Mater. Chem. A*, **4**(3), 991–999 (2016).
121. X. Leng, Q. Zeng, K.-H. Wu, I.R. Gentle and D.-W. Wang, Reduction-induced surface amorphization enhances the oxygen evolution activity in Co_3O_4, *RSC Adv.*, **5**(35), 27823–27828 (2015).
122. X. Deng, W.N. Schmidt, H. Tuysuz, Impacts of Geometry and Symmetry, and Morphology of Nanocast Co_3O_4 on Its Catalytic Activity for Water Oxidation, *Chem. Mater.*, **26**(21), 6127–6134 (2014).
123. C.-C. Lin, Y. Guo and J. Vela, Microstructure Effects on the Water Oxidation Activity of Co_3O_4/Porous Silica Nanocomposites, *ACS Catal.*, **5**(2), 1037–1044 (2015).
124. T.Y. Ma, S. Dai, M. Jaroniec and S.Z. Qiao, Metal–Organic Framework Derived Hybrid Co_3O_4-Carbon Porous Nanowire Arrays as Reversible Oxygen Evolution Electrodes, *J. Am. Chem. Soc.*, **136**(39), 13925–13931 (2014).

125. M.S. Burke, M.G. Kast, L. Trotochaud, A.M. Smith and S.W. Boettcher, Cobalt–iron (oxy) hydroxide oxygen evolution electrocatalysts: the role of structure and composition on activity and stability, and mechanism, *J. Am. Chem. Soc.*, **137**(10), 3638–3648 (2015).
126. J. Jia, X. Li and G. Chen, Stable spinel type cobalt and copper oxide electrodes for O_2 and H_2 evolutions in alkaline solution, *Electrochim. Acta*, **55**(27), 8197–8206 (2010).
127. T.W. Kim, M.A. Woo, M. Regis and K.-S. Choi, Electrochemical synthesis of spinel type $ZnCo_2O_4$ electrodes for use as oxygen evolution reaction catalysts, *J. Phys. Chem. Lett.*, **5**(13), 2370–2374 (2014).
128. C. Qiao, Y. Zhang, Y. Zhu, C. Cao, X. Bao and J. Xu, One-step synthesis of zinc–cobalt layered double hydroxide (Zn–Co-LDH) nanosheets for high-efficiency oxygen evolution reaction, *J. Mater. Chem. A*, **3**(13), 6878–6883 (2015).
129. F. Song and X. Hu, Ultrathin cobalt–manganese layered double hydroxide is an efficient oxygen evolution catalyst, *J. Am. Chem. Soc.*, **136**(47), 16481–16484 (2014).
130. M. Lyons, R. Doyle, I. Godwin, M. O'Brien and L. Russell, Hydrous nickel oxide: redox switching and the oxygen evolution reaction in aqueous alkaline solution, *J. Electrochem. Soc.*, **159**(12), H932–H944 (2012).
131. D. Cibrev, M. Jankulovska, T. Lana-Villarreal and R. Gómez, Oxygen evolution at ultrathin nanostructured Ni (OH) 2 layers deposited on conducting glass, *Int. J. Hydrogen Energ.*, **38**(6), 2746–2753 (2013).
132. M. Gao, W. Sheng, Z. Zhuang, Q. Fang, S. Gu, J. Jiang and Y. Yan, Efficient water oxidation using nanostructured α-nickel-hydroxide as an electrocatalyst, *J. Am. Chem. Soc.*, **136**(19), 7077–7084 (2014).
133. I. Godwin and M. Lyons, Enhanced oxygen evolution at hydrous nickel oxide electrodes via electrochemical ageing in alkaline solution, *Electrochem. Comm.*, **32**, 39–42 (2013).
134. L. Trotochaud, S.L. Young, J.K. Ranney and S.W. Boettcher, Nickel–iron oxyhydroxide oxygen-evolution electrocatalysts: The role of intentional and incidental iron incorporation, *J. Am. Chem. Soc.*, **136**(18), 6744–6753 (2014).
135. D.K. Bediako, B. Lassalle-Kaiser, Y. Surendranath, J. Yano, V.K. Yachandra and D.G. Nocera, Structure–activity correlations in a nickel–borate oxygen evolution catalyst, *J. Am. Chem. Soc.*, **134**(15), 6801–6809 (2012).
136. L. Trotochaud, J.K. Ranney, K.N. Williams and S.W. Boettcher, Solution-cast metal oxide thin film electrocatalysts for oxygen evolution, *J. Am. Chem. Soc.*, **134**(41), 17253–17261 (2012).
137. X. Li, F.C. Walsh, D. Pletcher and Nickel based electrocatalysts for oxygen evolution in high current density, alkaline water electrolysers, *Phys. Chem. Chem. Phys.*, **13**(3), 1162–1167 (2011).
138. C. Xiang, S.K. Suram, J.A. Haber, D.W. Guevarra, E. Soedarmadji, J. Jin and J.M. Gregoire, High-Throughput Bubble Screening Method for Combinatorial Discovery of Electrocatalysts for Water Splitting, *ACS Comb. Sci.*, **16**(2), 47–52 (2014).
139. M.W. Louie and A.T. Bell, An investigation of thin-film Ni–Fe oxide catalysts for the electrochemical evolution of oxygen, *J. Am. Chem. Soc.*, **135**(33), 12329–12337 (2013).
140. R.D. Smith, M.S. Prévot, R.D. Fagan, S. Trudel, C.P. Berlinguette, Water oxidation catalysis: electrocatalytic response to metal stoichiometry in amorphous metal oxide films containing iron and cobalt, and nickel, *J. Am. Chem. Soc.*, **135**(31), 11580–11586 (2013).
141. D.A. Corrigan, The catalysis of the oxygen evolution reaction by iron impurities in thin film nickel oxide electrodes, *J. Electrochem. Soc.*, **134**(2), 377–384 (1987).
142. M. Görlin, P. Chernev, J. Ferreira de Araújo, T. Reier, S.r. Dresp, B. Paul, R. Krähnert, H. Dau and P. Strasser, Oxygen Evolution Reaction Dynamics and Faradaic Charge Efficiency, and the Active Metal Redox States of Ni–Fe Oxide Water Splitting Electrocatalysts, *J. Am. Chem. Soc.*, **138**(17), 5603–5614 (2016).
143. D. Friebel, M.W. Louie, M. Bajdich, K.E. Sanwald, Y. Cai, A.M. Wise, M.-J. Cheng, D. Sokaras, T.-C. Weng and R. Alonso-Mori, Identification of highly active Fe sites in (Ni, Fe) OOH for electrocatalytic water splitting, *J. Am. Chem. Soc.*, **137**(3), 1305–1313 (2015).
144. X. Yu, M. Zhang, W. Yuan and G. Shi, A high-performance three-dimensional Ni–Fe layered double hydroxide/graphene electrode for water oxidation, *J. Mater. Chem. A*, **3**(13), 6921–6928 (2015).
145. X. Lu and C. Zhao, Electrodeposition of hierarchically structured three-dimensional nickel–iron electrodes for efficient oxygen evolution at high current densities, *Nat. Comm.*, **6**(2015).
146. L. Trotochaud, J.K. Ranney, K.N. Williams and S.W. Boettcher, Solution-Cast Metal Oxide Thin Film Electrocatalysts for Oxygen Evolution, *J Am Chem Soc*, **134**(41), 17253–17261 (2012).
147. A. Hellman and R.G.S. Pala, First-Principles Study of Photoinduced Water-Splitting on Fe_2O_3, *J. Phys. Chem. C*, **115**(26), 12901–12907 (2011).
148. S. Zou, M.S. Burke, M.G. Kast, J. Fan, N. Danilovic, S.W. Boettcher, Fe (Oxy) hydroxide Oxygen Evolution Reaction Electrocatalysis: Intrinsic Activity and the Roles of Electrical Conductivity and Substrate, and Dissolution, *Chem. Mater.*, **27**(23), 8011–8020 (2015).
149. B. Messaoudi, S. Joiret, M. Keddam and H. Takenouti, Anodic behaviour of manganese in alkaline medium, *Electrochim. Acta*, **46**(16), 2487–2498 (2001).
150. A. Bergmann, I. Zaharieva, H. Dau and P. Strasser, Electrochemical water splitting by layered and 3D cross-linked manganese oxides: correlating structural motifs and catalytic activity, *Energy Environ. Sci.*, **6**(9), 2745–2755 (2013).
151. K. Kishor, S. Saha, S. Sivakumar and R.G. Pala, Enhanced water oxidation activity of Co_3O_4 electrocatalyst on

earth abundant metal interlayered hybrid porous carbon support, *Chem Electro Chem*, Just Accepted (2016).

152. M. Gong, Y. Li, H. Wang, Y. Liang, J.Z. Wu, J. Zhou, J. Wang, T. Regier, F. Wei and H. Dai, An advanced Ni–Fe layered double hydroxide electrocatalyst for water oxidation, *J. Am. Chem. Soc.*, **135**(23), 8452–8455 (2013).
153. Y. Meng, W. Song, H. Huang, Z. Ren, S.-Y. Chen and S.L. Suib, Structure–Property Relationship of Bifunctional MnO_2 Nanostructures: Highly Efficient, Ultra-Stable Electrochemical Water Oxidation and Oxygen Reduction Reaction Catalysts Identified in Alkaline Media, *J. Am. Chem. Soc.*, **136**(32), 11452–11464 (2014).
154. R. Frydendal, M. Busch, N.B. Halck, E.A. Paoli, P. Krtil, I. Chorkendorff and J. Rossmeisl, Enhancing Activity for the Oxygen Evolution Reaction: The Beneficial Interaction of Gold with Manganese and Cobalt Oxides, *Chem Cat Chem*, **7**(1), 149–154 (2015).
155. L.C. Seitz, T.J. Hersbach, D. Nordlund and T.F. Jaramillo, Enhancement Effect of Noble Metals on Manganese Oxide for the Oxygen Evolution Reaction, *J. Phys. Chem. Lett*, **6**(20), 4178–4183 (2015).
156. K. Kishor, S. Saha, R.G. Pala and S. Sivakumar, Activity Trends of Co_3O_4 on Metallic Interlayers Supported on Porous Carbon Support, in: Meeting Abstracts, *Electrochem. Soc.*, 2016, pp. 1780–1780.
157. X. Lu and C. Zhao, Highly efficient and robust oxygen evolution catalysts achieved by anchoring nanocrystalline cobalt oxides onto mildly oxidized multiwalled carbon nanotubes, *J. Mater. Chem. A*, **1**(39), 12053–12059 (2013).
158. E. Antolini, Carbon supports for low-temperature fuel cell catalysts, *Appl. Catal. B: Environ.*, **88**(1), 1–24 (2009).
159. X. Lu and C. Zhao, Electrodeposition of hierarchically structured three-dimensional nickel-iron electrodes for efficient oxygen evolution at high current densities, *Nat. Comm.*, **6**, 1–7 (2015).
160. S. Yusuf and F. Jiao, Effect of the Support on the Photocatalytic Water Oxidation Activity of Cobalt Oxide Nanoclusters, *ACS Catal.*, **2**(12), 2753–2760 (2012).
161. P.W. Menezes, A. Indra, D. Gonzalez-Flores, N.R. Sahraie, I. Zaharieva, M. Schwarze, P. Strasser, H. Dau and M. Driess, High-Performance Oxygen Redox Catalysis with Multifunctional Cobalt Oxide Nanochains: Morphology-Dependent Activity, *ACS Catal.*, **5**(4), 2017–2027 (2015).
162. T. Kuwabara, B. Nishizawa, K. Nakamura, Y. Ikeda, T. Yamaguchi and K. Takahashi, Electrocatalytic activity of electrodeposited cobalt oxide films to produce oxygen gas from water, *J. Electroanal. Chem.*, **740**, 14–20 (2015).
163. Y. Zhao, B. Sun, X. Huang, H. Liu, D. Su, K. Sun and G. Wang, Porous graphene wrapped CoO nanoparticles for highly efficient oxygen evolution, *J. Mater. Chem. A*, **3**(10), 5402–5408 (2015).
164. H.-F. Wang, C. Tang and Q. Zhang, Towards superior oxygen evolution through graphene barriers between metal substrates and hydroxide catalysts, *J. Mater. Chem. A*, **3**(31), 16183–16189 (2015).
165. M. Zhang, Y.-L. Huang, J.-W. Wang and T.-B. Lu, A facile method for the synthesis of a porous cobalt oxide-carbon hybrid as a highly efficient water oxidation catalyst, *J. Mater. Chem. A*, **4**(5), 1819–1827 (2016).
166. N. Naseri, A. Esfandiar, M. Qorbani and A.Z. Moshfegh, Selecting Support Layer for Electrodeposited Efficient Cobalt Oxide/Hydroxide Nanoflakes to Split Water, *ACS Sustainable Chem. Engg.*, **4**(6), 3151–3159 (2016).
167. S. Du, Z. Ren, J. Zhang, J. Wu, W. Xi, J. Zhu and H. Fu, Co_3O_4 nanocrystal ink printed on carbon fiber paper as a large-area electrode for electrochemical water splitting, *Chem. Comm.*, **51**(38), 8066–8069 (2015).
168. A.P. Upadhyay, D.K. Behara, G.P. Sharma, G.P. Maurya, R.G.S. Pala and S. Sivakumar, Fabricating Appropriate Band-Edge-Staggered Heterosemiconductors with Optically Activated Au Nanoparticles via Click Chemistry for Photoelectrochemical Water Splitting, *ACS Sustainable Chem. Engg.*, **4**(9), 4511–4520 (2016).
169. D.K. Behara, G.P. Sharma, A.P. Upadhyay, M. Gyanprakash, R.G.S. Pala and S. Sivakumar, Synchronization of charge carrier separation by tailoring the interface of Si–Au–TiO_2 heterostructures via click chemistry for PEC water splitting, *Chem. Engg. Sci.*, **154**, 150–169 (2016).
170. A.P. Upadhyay, C.K. Rastogi, R.G.S. Pala and S. Sivakumar, Desorption retarded optically complemented multiple dye-sensitized photoelectrochemical water splitting system with enhanced performance, *Int. J. Hydrogen Energ.*, **41**(25), 10727–10736 (2016).
171. A.P. Upadhyay, D.K. Behara, G.P. Sharma, A. Bajpai, N. Sharac, R. Ragan, R.G.S. Pala and S. Sivakumar, Generic Process for Highly Stable Metallic Nanoparticle-Semiconductor Heterostructures via Click Chemistry for Electro/Photocatalytic Applications, *ACS Appl. Mater. Interfac.*, **5**(19), 9554–9562 (2013).
172. D.K. Behara, A.K. Ummireddi, V. Aragonda, P.K. Gupta, R.G.S. Pala and S. Sivakumar, Coupled optical absorption and charge carrier separation, and surface electrochemistry in surface disordered/hydrogenated TiO_2 for enhanced PEC water splitting reaction, *Phys. Chem. Chem. Phys.*, **18**(12), 8364–8377 (2016).
173. A.P. Upadhyay, D.K. Behara, G.P. Sharma, R.G.S. Pala and S. Sivakumar, Self-Directed Assembly of Nanoparticles, *Adv. Theranostic Mater.*, 297–343 (2015).
174. K. Kishor, A. Parashtekar, S. Saha, S. Sivakumar, J. Ramkumar and R.G.S. Pala, Rational design strategy for optimization of operating pressure to reduce contact resistance while preserving porosity of electrode, *J. Electrochem. Soc.*, Under review (2016).
175. A. Ursua, L.M. Gandia and P. Sanchis, Hydrogen production from water electrolysis: current status and future trends, *Proceed. IEEE*, **100**(2), 410–426 (2012).
176. K.E. Ayers, E.B. Anderson, C. Capuano, B. Carter, L. Dalton, G. Hanlon, J. Manco and M. Niedzwiecki, Research advances towards low cost, high efficiency PEM electrolysis, *ECS Trans.*, **33**(1), 3–15 (2010).

177. G.P. Gardner, Y.B. Go, D.M. Robinson, P.F. Smith, J. Hadermann, A. Abakumov, M. Greenblatt and G.C. Dismukes, Structural Requirements in Lithium Cobalt Oxides for the Catalytic Oxidation of Water, *Angew. Chem.*, **51**(7), 1616–1619 (2012).
178. D.M. Robinson, Y.B. Go, M. Mui, G. Gardner, Z. Zhang, D. Mastrogiovanni, E. Garfunkel, J. Li, M. Greenblatt and G.C. Dismukes, Photochemical Water Oxidation by Crystalline Polymorphs of Manganese Oxides: Structural Requirements for Catalysis, *J. Am. Chem. Soc.*, **135**(9), 3494–3501 (2013).
179. Z. Xu and J.R. Kitchin, Tuning oxide activity through modification of the crystal and electronic structure: from strain to potential polymorphs, *Phys. Chem. Chem. Phys.*, **17**(43), 28943–28949 (2015).
180. M. Pandey and R.G.S. Pala, Stabilization and growth of non-native nanocrystals at low and atmospheric pressures, *J. Chem. Phys.*, **136**(4), 044703 (2012).
181. M. Pandey and R.G.S. Pala, Stabilization of Rocksalt CdSe at Atmospheric Pressures via Pseudomorphic Growth, *J. Phys. Chem. C*, **117**(15), 7643–7647 (2013).
182. M. Pandey and R.G.S. Pala, Hydroxylation induced stabilization of near-surface rocksalt nanostructure on wurtzite ZnO structure, *J. Chem. Phys.*, **138**(22), 224701 (2013).
183. K.E. Ayers, C. Capuano and E.B. Anderson, Recent advances in cell cost and efficiency for PEM-based water electrolysis, *ECS Trans.*, **41**(10), 15–22 (2012).

Sulay Saha has done M.Tech in Chemical Engineering from IIT Kharagpur and currently pursuing Ph.D. in the department of Chemical Engineering, Indian Institute of Technology at Kanpur under the guidance of Dr. Sri Sivakumar and Dr. Raj Ganesh S. Pala of Chemical Engineering Department, IIT Kanpur. His research includes stabilization of desired phase and morphologies of nanocatalysts. Both experimental and computational tools are used for the study of nanocatalyst design and crystal growth. Presently he is involved in developing catalysts for water electrolysers and chlor-alkali industries.

Sri Sivakumar is an Associate Professor at the department of chemical engineering, Indian Institute of Technology at Kanpur. His research focuses on the development of various nanomaterials for various applications in particular drug delivery, bio-imaging, solar hydrogen generation, catalytic reactions, and solid state lightings. The research also focuses on growth and stabilization mechanism of nanomaterials whose understanding is essential in designing materials with multifunctional properties.

Koshal Kishor has done B.Tech in Chemical Engineering from UPTU Lucknow and M. Tech in High Energy Materials from DIAT/DRDO and currently pursuing Ph.D. in the department of Chemical Engineering, Indian Institute of Technology at Kanpur under esteemed guidance of Dr. Raj Ganesh S. Pala of Chemical Engineering Department, IIT Kanpur. He has done work in the field of electrochemistry especially for the water electrolyser (Design of electrocatalysts, membrane and membrane electrode assembly). Presently he is working on design of electrode for chlor-alkali industries. He is also working as a Guest Faculty at HBTU Kanpur.

Raj Ganesh S. Pala works in the broad area of electrochemical and reaction engineering with the current focus being electrocatalysis and photoelectrocatalysis of water splitting and reduction of CO_2, models for crystal growth, selectivity in organic electrochemistry/heterogeneous catalysis, electrode design for batteries and solar based membrane distillation. The research group aims to elucidate concepts that aid in designing functional materials and this often involves a semi-quantitative description of phenomena that span a wide range of length and time scales. In this context, analysis is performed via electrochemical and catalytic rate measurements, spectroscopy, quantum chemical density functional simulations and other computational techniques.